Department of Physics and Astronomy
University of Heidelberg

Master Thesis in Physics
submitted by

Linda Angenoorth

born in Munich (Germany)

2017

Bogoliubov theory of quantum fluctuations around acoustic black hole horizons in a two component Bose Einstein condensate

This Master Thesis has been carried out by Linda Angenoorth at the
Institute for Theoretical Physics in Heidelberg
under the supervision of
Prof. Dr. Thomas Gasenzer

Bogoliubov Theorie von Quantenfluktuationen um den Horizont eines akkustischen schwarzen Lochs in einem zweikomponentigen Bose Einstein Kondensat

Wir betrachten eine einfache Realisierung eines Ereignishorizontes im Fluss eines eindimensionalen, zweikomponentigen Bose Einstein Kondensates. Unsere Rechnungen basieren ausschließlich auf der mikroskopischen Bogoliubov Theorie für Bose Einstein Kondensate, in der symmetrische und antisymmetrische Freiheitsgrade entkoppeln. Auf die Gravitationsanalogie beziehen wir uns nur, um die akustische Metrik zu berechnen. Wir untersuchen das Signal in der zwei-Punkt Dichtekorrelation, welches mit dem Analog von spontaner Hawkingstrahlung assoziiert wird, in verschiedenen Konfigurationen, in welchen ein Horizont nur in den antisymmetrischen Freiheitsgraden auftritt, während der Fluss in den symmetrischen Freiheitsgraden überall unter Schallgeschwindigkeit bleibt. Explizite Berechnungen zeigen, dass das Hawkingsignal nur in den antisymmetrischen Freiheitsgraden auftritt. Wir beobachten auch ein Hawking-artiges Korrelationssignal in einer Konfiguration, in welcher die Quasiteilchen eine effektive Masse haben.

Bogoliubov theory of quantum fluctuations around acoustic black hole horizons in a two component Bose Einstein condensate

We consider a simple realisation of an event horizon in the flow of a one-dimensional two-component Bose Einstein condensate. Our calculations are completely based on the microscopic Bogoliubov theory of dilute Bose Einstein condensates where symmetric and anti-symmetric degrees of freedom decouple. Reference to the gravitational analogy is only made to calculate the acoustic metric. We study the two-point density correlation signal associated with the analogue of spontaneous Hawking emission in several configuration, where a horizon only occurs in the anti-symmetric regime, while the flow stays overall subsonic in the symmetric regime. Explicit calculations show that the Hawking signal is only present in the anti-symmetric regime. We also find a Hawking-like long-range correlation signal in a configuration, where the quasi-particles have an effective mass.

Contents

List of Figures

1 Introduction

Einstein's theory of general relativity predicts that a sufficiently compact mass can deform spacetime to form a black hole, an object with such a strong gravitational field that nothing, not even light, can escape from it once it has crossed its event horizon. Therefore, for a long time black holes were considered to be totally "black" and only indirectly observable through the behaviour of matter orbiting around it outside the horizon.
In 1974 Stephen Hawking showed [1, 2] that if one takes quantum mechanics into account, stationary black holes are no longer "black" but emit a steady flux of thermal radiation as if they where black bodies with a temperature inversely proportional to their masses. Though due to the in general extremely high mass of a black hole this temperature is many orders of magnitude smaller than the $2.7K$ of the cosmic microwave background, making it virtually impossible to observe the Hawking signal. However because of the radiation black holes are expected to lose mass which would increase the rate of emission. In his letter Stephen Hawking predicts the lifetime of a black hole to be of the order $10^{71}\left(M/M_{\odot}\right)^{3} s$ [1], which is, for a black hole of solar mass, much longer than the current age of the universe. But a much smaller black hole, formed by the fluctuations in the early stages in the live of the universe [3], might exist. Such a primordial black hole would have almost completely evaporated by today and the temperature of its Hawking radiation would be high enough to be actually observable.
However, to this date Hawking radiation is unobserved in space. Yet in recent years the possibility of creating analogue black holes in the lab and observing the Hawking signal in this analogue models of gravity became very real.
In 1981 W. G. Unruh proposed an analogy between sound propagation in non-homogeneous media and light propagation in curved space-times. He predicted, that in a transsonic fluid flow a thermal spectrum of sound waves should be emitted. Indeed, the point of transition from a subsonic upstream to a supersonic downstream flow acts on sound waves as an analogue of an event horizon. If the flow remains stationary across such a sonic horizon, one expects to obtain a thermal flux of phonons with a temperature of $k_{\mathbf{B}}T = \hbar\kappa/2\pi$, where κ is the gradient of the flow velocity evaluated at the hori-

zon. Analogue to the arguments which lead to gravitational black-hole evaporation [2], quantum virtual particles can tunnel out near the sonic horizon and are then separated by the background flow. This gives rise to correlated currents emitted away from the horizon, both inside and outside of the sonic black hole.

In [4] W. G. Unruh gives a nice colourful introduction to the acoustic analogy about hyper-intelligent fish living in the oceans of Discwold, the location of Terry Pratchetts Discworld series of novels. The waterfall at the edge of Discwordl is called Rimfall and for the hyper-intelligent fish it was a boundary, a horizon, beyond which nothing could be heard. The fish realised, that the screams of those who travelled to close to this horizon, were infinitely bass shifted arbitrarily far into the future, though in no case could anything ever be heard from beyond the horizon. W. G. Unruh actually first used this analogy in a colloquium at Oxford University in 1972 to explain classical black holes. Years later, in 1981, he realised that the equations of motion for sound waves and those near a black hole are identical and that the quantisation of the sound waves would produce thermal radiation just as Hawking had predicted for black holes [1]. Since then many different setups that behave in the same way were proposed.

In the last decade sonic horizons have been realised in different experimental configurations. In [5, 6] a dump hole configuration for surface waves on a tank of moving water was realised and the observation of conversion of positive frequency waves into negative frequency waves was reported. This can be considered as a classical analogue of the Hawking effect [7]. Though note that in this case the Hawking radiation results from a disturbance external to the system. Therefore the observed effect is a stimulated emission. Also among the experimental configurations where a sonic horizon was realised are ultrashort pulses moving in optical fibers [8] or in a dielectric medium [9] and laser propagating in a non-linear luminous liquid [10]. Other realisations of an acoustic event horizon were proposed in theoretical works. For instance using a ring-shaped chain of trapped ions [11], an electromagnetic wave guide [12], graphene [13, 14] or edge modes of the filling fraction $\nu = 1$ quantum Hall system [15].

The specific implementation of the acoustic analogy using Bose Einstein condensates was first proposed by Garay *et al.*[16], followed by many others [17, 18, 19, 20, 21, 22, 23, 24, 25, 26, 27, 28]. In [29, 30, 31, 32] an exciton-polariton superfluid was considered, which is a likely candidate for experimental observation in the near future. Dilute Bose Einstein condensates have nice properties from the theoretical as well as the experimental point of view. From the first, the equations of motion for the condensate and the phonons, as well as the approximations they involve, are well understood [33]. And from the second, the advances in the cooling and manipulation of ultracold atomic gases as well as the

control of their physical properties in the last years have been great. The realisation of an acoustic horizon in the flow of a Bose Einstein condensate past an obstacle has been reported in [34] and last year Jeff Steinhauer claimed he had observed quantum Hawking radiation and its entanglement [35].
In [24, 36] two point density correlations have been proposed as an observable quantity to identify the spontaneous Hawking emission. In contrast to the gravitational case, it is possible in the analogy to extract information from the interior of an acoustic black hole. Therefore measuring a correlation signal between the currents emitted inside and outside of the black hole can give insight on the Hawking effect. This correlation signal appears to be only slightly affected by the thermal noise [26] hence seems to be a more efficient measure of the Hawking effect than direct detection of the Hawking phonons.

In this thesis we study the signatures of Hawking radiation in a two-component Bose Einstein condensate. Such a system sustains two types of elementary excitations, both with different long-wavelength velocities. This makes it possible to realise a unique configuration, where a sonic horizon only occurs for one of the elementary excitations but not for the other. We consider such a configuration for different sets of coupling parameters. This gives us the opportunity to go beyond the usual Hawking effect of massless phonons and consider a Hawking effect of massive particles.
Our calculations are based on a direct application of the standard Bogoliubov theory of dilute condensates. A reference to the gravitational analogy is only made when we derive the acoustic metric. To simplify matters we consider a step-like configuration where the transition from the subsonic to the supersonic region happens on a very short length scale. Despite the formally infinite surface gravity of this configuration, there is still a thermal-like Hawking emission at a temperature fixed by the healing length.

2 Theoretical background

2.1 Bogoliubov theory of a two-component Bose Einstein condensate with a background flow

Throughout this whole thesis we use a unit system with $\hbar = 1$.
Two coupled Bose Einstein condensates in one spacial dimension can be described by the Hamiltonian

$$\begin{aligned}\mathcal{H} = \int dx \Bigg\{ & \sum_{j=1,2} \psi_j^\dagger \left[-\frac{1}{2m}\partial_x^2 + \left(V(x) - \mu\right) \right] \psi_j \\ & -J\left(\psi_1^\dagger \psi_2 + \psi_2^\dagger \psi_1\right) + \sum_{i,j=1,2} \frac{g_{\mathrm{ij}}}{2} \psi_i^\dagger \psi_i \psi_j^\dagger \psi_j \Bigg\},\end{aligned} \tag{2.1}$$

where $V(x)$ is an external potential, μ the chemical potential, J the tunnel coupling and g_{ij} are the inter and intra species coupling. We set $g_{11} = g_{22} = g$ and $g_{12} = g_{21} = \alpha g$. We also assume both component to have equal atomic mass m. The annihilation and creation operators $\psi_{1,2}$ and $\psi_{1,2}^\dagger$ of the respective condensates fulfil bosonic commutation relations

$$\left[\psi_i(x,t), \psi_j^\dagger(x',t)\right] = \delta_{\mathrm{ij}}\delta(x - x'), \tag{2.2}$$

all others vanish.

A set of two coupled equations of motion for the condensates can be derived by using the Heisenberg equation

$$i\partial_t \psi_j = \left[\psi_j, H\right]. \tag{2.3}$$

Adopting the Madelung representation, that is expressing the bosonic field operators in terms of their real-valued density $n(x)$ and phase $\theta(x)$ fields, gives us

$$\psi_j \to \sqrt{n_j(x)}e^{i\theta_j(x)}, \tag{2.4}$$

where n_j and θ_j are required to obey the commutation relation $\left[n_i(x,t), \theta_j(x',t)\right] = i\delta_{ij}\delta(x-x')$.
This leads to a set of four coupled equations of motion for n_1,n_2,θ_1 and θ_2,

$$\partial_t n_i = -\frac{1}{m}\partial_x\left[n_i\partial_x\theta_i\right] + 2J\sqrt{n_i n_j}\sin\left(\theta_i-\theta_j\right), \tag{2.5a}$$

$$\begin{aligned}\partial_t\theta_i = {} & \frac{1}{2m}\frac{\partial_x^2\sqrt{n_i}}{\sqrt{n_i}} - \frac{1}{2m}\left(\partial_x\theta_i\right)^2 - \left[V(x)-\mu\right] \\ & + J\sqrt{\frac{n_j}{n_i}}\cos\left(\theta_i-\theta_j\right) - gn_i - \alpha g n_j,\end{aligned} \tag{2.5b}$$

with $i,j\in\{1,2\}$ and $i\neq j$.

As we are in the quasi-condensate regime, Bogoliubov theory is the way to go. We therefor assume a smooth background for our fields and introduce small fluctuations on them,

$$n_i(x,t) = n_0(x) + \delta n_i(x,t), \tag{2.6a}$$

$$\theta_i(x,t) = \theta_0(x) + \delta\theta_i(x,t). \tag{2.6b}$$

We assume the backgrounds to be equal for both condensates, that is $(n_0)_1 = (n_0)_2$ and $(\theta_0)_1 = (\theta_0)_2$.
With $\theta_0(x)$ we also introduced the background flow of our system, which is defined as

$$v(x) := \frac{\partial_x\theta_0(x)}{m}. \tag{2.7}$$

The background velocity is also equal for both components of our Bose gas.

Linearizing equations (2.5) we find in lowest order

$$\left[-\frac{1}{2m}\partial_x^2\sqrt{n_0} + \frac{1}{2}mv^2 + V(x) - (J+\mu) + g(1+\alpha)n_0\right]\sqrt{n_0} = 0, \tag{2.8}$$

which is the usual Gross-Pitaevskii equation with an additional kinetic energy term $\frac{1}{2}mv^2$ due to the background velocity and a shifted chemical potential due to the tunnel coupling J. We also find

$$\partial_x \left[n_0 v\right] = 0, \tag{2.9}$$

which is the continuity equation.

For further calculations it is convenient to work in the decoupled symmetric (+) and anti-symmetric (−) degrees of freedom,

$$\delta n_+ = \delta n_1 + \delta n_2, \qquad \delta\theta_+ = \frac{\delta\theta_1 + \delta\theta_2}{2}, \tag{2.10a}$$

$$\delta n_- = \frac{\delta n_1 - \delta n_2}{2}, \qquad \delta\theta_- = \delta\theta_1 - \delta\theta_2. \tag{2.10b}$$

One should notice, that the linearised equations in the symmetric and anti-symmetric degrees of freedom only decouple, because we chose a symmetric configuration with $m_1 = m_2$, $(n_0)_1 = (n_0)_2$, etc. Without these assumptions the equations of the two regimes would stay coupled.

In the symmetric degrees of freedom we find in first order

$$\partial_t \delta n_+ = -\partial_x \left[\delta n_+ v + \frac{2n_0}{m}\partial_x \delta\theta_+\right], \tag{2.11a}$$

$$\partial_t \delta\theta_+ = -v\partial_x \delta\theta_+ + \frac{1}{2m}\frac{1}{4n_0}\partial_x \left[n_0 \partial_x \left(\frac{\delta n_+}{n_0}\right)\right] - \frac{g}{2}\left(1+\alpha\right)\delta n_+, \tag{2.11b}$$

and for the anti-symmetric degrees of freedom we find

$$\partial_t \delta n_- = -\partial_x \left[\delta n_- v + \frac{n_0}{2m}\partial_x \delta\theta_-\right] + 2Jn_0\delta\theta_-, \tag{2.12a}$$

$$\partial_t \delta\theta_- = -v\partial_x \delta\theta_- + \frac{1}{2m}\frac{1}{n_0}\partial_x \left[n_0 \partial_x \left(\frac{\delta n_-}{n_0}\right)\right] - 2J\frac{\delta n_-}{n_0} - 2g\left(1-\alpha\right)\delta n_-. \tag{2.12b}$$

We will now consider a region in which the condensate is homogeneous (with constant n_0 and v, and $V(x) = 0$). Then the solutions can be expanded in terms of plane waves

$$\delta n_+ = Ae^{i(kx-\omega_+ t)}, \qquad \delta\theta_+ = Be^{i(kx-\omega_+ t)}, \tag{2.13a}$$
$$\delta n_- = Ce^{i(kx-\omega_- t)}, \qquad \delta\theta_- = De^{i(kx-\omega_- t)}, \tag{2.13b}$$

where A, B, C and D are constant amplitudes. Substituting these into equations (2.11) and (2.12) we find

$$\begin{pmatrix} i(\omega_+ - vk) & 4\left[\frac{1}{2m}k^2\right] \\ \frac{1}{4}\left[\frac{1}{2m}k^2 + 2gn_0(1+\alpha)\right] & -i(\omega_+ - vk) \end{pmatrix} \begin{pmatrix} A \\ B \end{pmatrix} = 0, \tag{2.14}$$

for the symmetric degrees of freedom and

$$\begin{pmatrix} i(\omega_- - v_+ k) & \left[\frac{1}{2m}k^2 + 2J\right] \\ \left[\frac{1}{2m}k^2 + 2J + 2gn_0(1-\alpha)\right] & -i(\omega_- - v_+ k) \end{pmatrix} \begin{pmatrix} C \\ D \end{pmatrix} = 0. \tag{2.15}$$

for the anti-symmetric degrees of freedom. In order for these equations to have nontrivial solutions the determinants of the matrices must vanish. This leads us to the dispersion relations

$$(\omega_+ - vk)^2 = \frac{1}{2m}k^2\left[\frac{1}{2m}k^2 + 2gn_0(1+\alpha)\right], \tag{2.16a}$$
$$(\omega_- - vk)^2 = \left[\frac{1}{2m}k^2 + 2J\right]\left[\frac{1}{2m}k^2 + 2gn_0(1-\alpha) + 2J\right]. \tag{2.16b}$$

The right sides of the dispersion relations (2.16) are just the standard Bogoliubov dispersion relation and the gaped dispersion relation respectively as we know it from a two component Bose gas, while the left sides show an energy shift due to the background flow of velocity v. They show the usual phononic behaviour in the low k limit and become quadratic for large k. A non-zero tunnel coupling $J \neq 0$ can open a gap in (2.16b) and modify the linear behaviour of small k.

In general the dispersion relation can be written as [37]

$$\Omega^2 = \omega_0^2 + c^2 k^2 + a_4 k^4 + ... \tag{2.17}$$

where Ω is the frequency in the co-moving reference frame, ω_0 is proportional to an effective mass, c is the velocity of sound and a_4 are higher order corrections which go beyond the hydrodynamic approximation.
With our dispersion relations (2.16) this gives us two different velocities of sound for the symmetric and the anti-symmetric degrees of freedom, respectively

$$c_+^2 = \frac{g n_0 (1+\alpha)}{m}, \tag{2.18a}$$
$$c_-^2 = \frac{g n_0 (1-\alpha) + 2J}{m}. \tag{2.18b}$$

Following [38] we are now introducing the new variables $\delta\tilde{n}_a = \delta n_a/\sqrt{n_0}$ and $\delta\tilde{\theta}_a = \delta\theta_a\sqrt{n_0}$ with $a \in \{+,-\}$, to simplify the notation. Now the equations of motion (2.11) and (2.12) take the compact form

$$[\partial_t + \mathcal{V}]\,\delta\tilde{n}_a = \lambda_a \left[\tilde{H} - \chi_a - g n_0 + g\alpha n_0\right]\delta\tilde{\theta}_a, \tag{2.19a}$$
$$[\partial_t + \mathcal{V}]\,\delta\tilde{\theta}_a = -\frac{1}{\lambda_a}\left[\tilde{H} + -\chi_a + g n_0 + \zeta_a g\alpha n_0\right]\delta\tilde{n}_a, \tag{2.19b}$$

with $\lambda_+ = 4$, $\chi_+ = \mu + J - \frac{1}{2}mv^2$, $\zeta_+ = 3$ for the symmetric degrees of freedom, $\lambda_- = 1$, $\chi_- = \mu - J - \frac{1}{2}mv^2$, $\zeta_- = -1$ for the anti-symmetric degrees of freedom, $\tilde{H} = -\frac{1}{2m}\partial_x^2 + V(x) + 2gn_0$ and $\mathcal{V} = \frac{\partial_x v}{2} + v\partial_x$. For a configuration with a constant background velocity $\mathcal{V}$ simplifies to $v\partial_x$. One should also notice, that the above equations (2.19) also describe a normal one-component Bose gas with a background velocity v for $\lambda_1 = 2$, $\chi_1 = \mu - \frac{1}{2}mv^2$ and $\zeta_1 = \alpha = 0$. By additionally setting $v = 0$ we would get the usual equations for a single Bose gas at rest.

In order to diagonalize the second order Hamiltonian within the quasi-particle basis,

$$\mathcal{H}_a^{(2)} = \sum_k \omega_{a,k}\hat{b}_{a,k}\hat{b}_{a,k}^\dagger, \tag{2.20}$$

we use the Bogoliubov expansion of the hydrodynamic variables [38, 39]

$$\delta\tilde{n}_a(x,t) = \frac{\sqrt{\lambda_a}}{2}\sum_k \left[f^+_{a,k}e^{-i\omega_{a,k}t}\hat{b}_k + \left(f^+_{a,k}\right)^* e^{i\omega_{a,k}}\hat{b}^\dagger_k\right], \tag{2.21a}$$

$$\delta\tilde{\theta}_a(x,t) = \frac{1}{i\sqrt{2\lambda_a}}\sum_k \left[f^-_{a,k}e^{-i\omega_{a,k}t}\hat{b}_k - \left(f^-_{a,k}\right)^* e^{i\omega_{a,k}}\hat{b}^\dagger_k\right]. \tag{2.21b}$$

The operators $\hat{b}^\dagger_k$ and $\hat{b}_k$ correspond to the creation and annihilation operators for bosonic quasi-particle excitations and fulfil bosonic commutation relations

$$\left[\hat{b}_k, \hat{b}^\dagger_{k'}\right] = \delta_{kk'}, \tag{2.22}$$

all others vanish.
The modefunctions $f^\pm_{a,k}$ relate to the normal Bogoliubov mode functions $u_{a,k}$ and $v_{a,k}$ by $f^\pm_{a,k} = u_{a,k} \pm v_{a,k}$. The normal mode functions $u_{a,k}$ and $v_{a,k}$ are normalised by $\int dx \left[|u_{a,k}|^2 - |v_{a,k}|^2\right] = \pm 1$, therefore the $f^\pm_{a,k}$ normalise as

$$\frac{1}{2}\int dx \left[\left(f^+_{a,k}\right)^*\left(f^-_{a,k'}\right) + \left(f^-_{a,k}\right)^*\left(f^+_{a,k'}\right)\right] = \pm\delta_{k,k'}. \tag{2.23}$$

Putting the Bogoliubov expansion (2.21) into equations (2.19) gives us the equations for the eigenfunctions $f^\pm_{a,k}$ and their corresponding eigenvalues $\Omega_{a,k}$ of the excitations

$$\Omega_{a,k}\begin{pmatrix} f^+_{a,k} \\ f^-_{a,k}\end{pmatrix} = \mathcal{L}_a \begin{pmatrix} f^+_{a,k} \\ f^-_{a,k}\end{pmatrix}, \tag{2.24}$$

with $\Omega_{a,k} = \omega_{a,k} + i\mathcal{V}$ and

$$\mathcal{L}_a = \begin{pmatrix} 0 & \tilde{H} - \chi_a - gn_0 + g\alpha n_0 \\ \tilde{H} - \chi_a + gn_0 + \zeta_a g\alpha n_0 & 0\end{pmatrix}. \tag{2.25}$$

For an homogeneous condensate (with constant n_0 and v, and $V(x) = 0$) the solutions

for the Bogoliubov modes are well known [38, 39]. In the symmetric regime we have

$$f^{+}_{+,k} = e^{ikx} F^{+}_{+,k} = e^{ikx} \frac{\frac{k^2}{2m}}{\sqrt{\left| Re\left(\frac{k^2}{2m}\Omega^{*}_{+,k}\right)\right|}}, \tag{2.26a}$$

$$f^{-}_{+,k} = e^{ikx} F^{-}_{+,k} = e^{ikx} \frac{\Omega_{+,k}}{\sqrt{\left| Re\left(\frac{k^2}{2m}\Omega^{*}_{+,k}\right)\right|}}, \tag{2.26b}$$

and in the anti-symmetric

$$f^{+}_{-,k} = e^{ikx} F^{+}_{-,k} = e^{ikx} \frac{\frac{k^2}{2m} + 2J}{\sqrt{\left| Re\left(\left(\frac{k^2}{2m} + 2J\right)\Omega^{*}_{-,k}\right)\right|}}, \tag{2.27a}$$

$$f^{-}_{-,k} = e^{ikx} F^{-}_{-,k} = e^{ikx} \frac{\Omega_{-,k}}{\sqrt{\left| Re\left(\left(\frac{k^2}{2m} + 2J\right)\Omega^{*}_{-,k}\right)\right|}}, \tag{2.27b}$$

with $\Omega_{\pm,k} = \omega_{\pm,k} - vk$.
We chose the normalisation factors $\left| Re\left(\frac{k^2}{2m}\Omega^{*}_{+,k}\right)\right|^{-1/2}$ and $\left| Re\left(\left(\frac{k^2}{2m} + 2J\right)\Omega^{*}_{-,k}\right)\right|^{-1/2}$ such that the normalisation condition (2.23) also holds for complex k. It is easy to check that real valued k will yield the usual expression as in [38, 39]

Now looking at the norm (2.23) we see that, as expected, states with a positive norm correspond to the branch of the dispersion relation with a positive co-moving frequency, while the negative norm states correspond to the branch with a negative co-moving frequency. Furthermore for any positive norm branch with frequency ω and corresponding wavevector k, there is a negative norm branch with frequency $-\omega$ and corresponding wavevector $-k$. Thus by using both positive and negative norm states, we can replace the sum over all wavevektors k in (2.21) by an integral over ω, restricted to $\omega \geq 0$.
The transformation from k to ω gives us an extra factor of $\left|\frac{dk}{d\omega}\right|$ in (2.21), which is just

the inverse group velocity $v_g = \frac{d\omega}{dk}$. Therefore our rescaled modefunctions are

$$f^{+}_{+,\ell}(\omega) = e^{ik_\ell x} F^{+}_{+,\ell}(\omega) = e^{ik_\ell x} \frac{\frac{k_\ell^2}{2m}}{\sqrt{|v_g(k_\ell)| \left| Re\left(\frac{k_\ell^2}{2m}\Omega^*_{+,\ell}\right)\right|}}, \tag{2.28a}$$

$$f^{-}_{+,\ell}(\omega) = e^{ik_\ell x} F^{-}_{+,\ell}(\omega) = e^{ik_\ell x} \frac{\Omega_{+,\ell}}{\sqrt{|v_g(k_\ell)| \left| Re\left(\frac{k_\ell^2}{2m}\Omega^*_{+,\ell}\right)\right|}}, \tag{2.28b}$$

for the symmetric degrees of freedom and

$$f^{+}_{-,\ell}(\omega) = e^{ik_\ell x} F^{+}_{-,\ell}(\omega) = e^{ik_\ell x} \frac{\frac{k_\ell^2}{2m} + 2J}{\sqrt{|v_g(k_\ell)| \left| Re\left(\left(\frac{k_\ell^2}{2m} + 2J\right)\Omega^*_{-,\ell}\right)\right|}}, \tag{2.29a}$$

$$f^{-}_{-,\ell}(\omega) = e^{ik_\ell x} F^{-}_{-,\ell}(\omega) = e^{ik_\ell x} \frac{\Omega_{-,\ell}}{\sqrt{|v_g(k_\ell)| \left| Re\left(\left(\frac{k_\ell^2}{2m} + 2J\right)\Omega^*_{-,\ell}\right)\right|}}, \tag{2.29b}$$

for the anti-symmetric ones. Where ℓ labels one of the four possible k-roots for a fixed ω. The rescaled operators are $\hat{b}_k = \hat{b}_{k_\ell}(\omega)/\sqrt{|v_g(k_\ell)|}$.
The modefunctions now normalise to

$$\begin{aligned} &\frac{1}{2}\int dx \left[\left(f^{+}_{a,k}(\omega)\right)^* \left(f^{-}_{a,k'}(\omega')\right) + \left(f^{-}_{a,k}(\omega)\right)^* \left(f^{+}_{a,k'}(\omega')\right)\right] \\ &\qquad = \pm\delta_{k,k'}\delta(\omega - \omega'). \end{aligned} \tag{2.30}$$

2.2 The acoustic metric

After applying Bogoliubov theory on a mostly general configuration of a two-component Bose gas with a background flow, we will now do a little excursion to analogue gravity. In the single Bose gases usually used as an analogue space-time the equations describing the propagation of long wavelength sound waves in the moving gas can be rewritten in terms of a massless scalar field propagation in curved space-time with an acoustic metric [40]. However, the two component condensate we are working with also holds the possibility of investigating the analogue model of massive particles interacting with

a scalar field in curved space-time since the gap in the dispersion relation in the anti-symmetric degrees of freedom causes an effective mass. In this section we will derive the two acoustic metrics occurring in our system.

In order to derive these we need to work in 3 spacial dimensions since the metric can not be defined in only one spacial dimension. We also only consider our system on length scales much larger then the healing length $\xi_{\pm} = \frac{1}{mc_{\pm}}$ such that the hydrodynamic approximation holds. In the hydrodynamic limit we only keep terms up to second order in k. For our equations this means that we only keep first and second derivatives.

In the symmetric degrees of freedom the application of the hydrodynamic approximation is pretty straight forward. Here it means that we can just neglect the quantum pressure term [41], which is the second term on the right side of equation (2.11b). Thus equation (2.11b) can be rewritten as

$$\begin{aligned} \delta n_{+} &= -\frac{2}{g\,(1+\alpha)}\left[v\nabla_{x}\delta\theta_{+} + \partial_{t}\delta\theta_{+}\right] \\ &= -\frac{2n_{0}}{mc_{+}^{2}}\left[v\nabla_{x}\delta\theta_{+} + \partial_{t}\delta\theta_{+}\right]. \end{aligned} \tag{2.31}$$

Now inserting the above expression for δn_{+} into equation (2.11a) yields the wave equation for the phase perturbations $\delta\theta_{+}$

$$-\left(\partial_{t} + \nabla_{x}v\right)\frac{n_{0}}{mc_{+}^{2}}\left(\partial_{t} + v\nabla_{x}\right)\delta\theta_{+} + \nabla_{x}\left(\frac{n_{0}}{m}\nabla_{x}\delta\theta_{+}\right) = 0. \tag{2.32}$$

Following [41, 42] this can also be written in matrix form

$$\partial_{\mu}\left(f^{\mu\nu}\partial_{\nu}\delta\theta_{+}\right) = 0, \tag{2.33}$$

with

$$f^{\mu\nu} = \frac{n_{0}}{c_{+}^{2}}\begin{pmatrix} -1 & -v^{j} \\ -v^{i} & c_{+}^{2}\delta^{ij} - v^{i}v^{j} \end{pmatrix}. \tag{2.34}$$

Now the curved space-time d'Alembertian operator for a massless scalar field in a standard pseudo-Riemannian geometry is

$$\Box := \frac{1}{\sqrt{-g}}\partial_{\mu}\left(\sqrt{-g}g^{\mu\nu}\partial_{\nu}\right), \tag{2.35}$$

where $g_{\mu\nu}$ is the metric, $g^{\mu\nu}$ its inverse and $g = \det\left(g_{\mu\nu}\right)$.
By identifying

$$f^{\mu\nu} = \sqrt{-g} g^{\mu\nu}, \tag{2.36}$$

we can rewrite equation (2.33) in the form of a curved space wave equation

$$\Box \delta\theta_+ = 0. \tag{2.37}$$

The definition (2.36) implies that

$$\det\left(f^{\mu\nu}\right) = \sqrt{-g}^4 \frac{1}{g} = g = \frac{-n_0^4}{c_+^2}. \tag{2.38}$$

Thus the inverse acoustic metric is

$$g^{\mu\nu} = \frac{1}{n_0 c_+} \begin{pmatrix} -1 & -v^j \\ -v^i & c_+^2 \delta^{ij} - v^i v^j \end{pmatrix}. \tag{2.39}$$

The acoustic metric itself (in the symmetric degrees of freedom) is now determined by inverting $g^{\mu\nu}$

$$g_{\mu\nu} = \frac{n_0}{c_+} \begin{pmatrix} -\left(c_+^2 - v^2\right) & -v^j \\ -v^j & \delta^{ij} \end{pmatrix}. \tag{2.40}$$

The acoustic line element can be expressed as

$$ds^2 = \frac{n_0}{c_+} \left[-c_+^2 dt^2 + \left(dx^i - v^i dt\right) \delta_{ij} \left(dx^j - v^j dt\right)\right]. \tag{2.41}$$

Now, for the anti-symmetric degrees of freedom the derivation of the acoustic metric is a bit more tricky. To apply the hydrodynamic approximation we cannot just neglect the quantum pressure term because by doing so we would also neglect some terms that are second order in k. Therefore the first part of the calculations are a bit more lengthy here.

Rewriting equation (2.12b) such that δn_- is isolated on one side of the equation like we did with equation (2.11b), is not possible here. Though we can rewrite it as

$$\delta n_- = -\frac{n_0}{2\left(g n_0 \left(1 - \alpha\right) + J\right)} \left[\partial_t \delta\theta_- + v \nabla_x \delta\theta_- - \frac{1}{2m} \frac{1}{n_0} \nabla_x \left[n_0 \nabla_x \left(\frac{\delta n_-}{n_0}\right)\right]\right]. \tag{2.42}$$

Next we take the time derivative of equation (2.12b) and insert equation (2.12a). Now using equation (2.42) on the resulting equation and thereby only keeping derivatives up to second order gives us

$$\begin{aligned} &-\left(\partial_t + \nabla_x v\right) \frac{n_0}{m c_-^2} \left(\partial_t + v\nabla_x\right) \delta\theta_- + \nabla_x \left(\frac{n_0}{m} \nabla_x \delta\theta_-\right) \\ &- 4\frac{n_0}{m c_-^2} J \left(g n_0 \left(1-\alpha\right) + J\right) \delta\theta_- = 0. \end{aligned} \tag{2.43}$$

As we did before in the symmetric degrees of freedom, this can also be written in matrix form [37]

$$\partial_\mu \left(f^{\mu\nu} \partial_\nu \delta\theta_+\right) - \tilde{V} = 0, \tag{2.44}$$

with $\tilde{V} = -4\frac{n_0}{m c_-^2} J \left(g n_0 \left(1-\alpha\right) + J\right)$ and

$$f^{\mu\nu} = \frac{n_0}{c_-^2} \begin{pmatrix} -1 & -v^j \\ -v^i & c_-^2 \delta^{ij} - v^i v^j \end{pmatrix}. \tag{2.45}$$

Now following the procedure above we can rewrite equation (2.44) as

$$\left(\Box - V\right) \delta\theta_- = 0, \tag{2.46}$$

with $V = \frac{\tilde{V}}{\sqrt{-g}}$. Note that $V = \frac{1}{n_0 c_-} \omega_0^2$ with ω_0 being defined in equation (2.17), is effectively a mass with $m_{\text{eff}}^2 = \frac{\omega_0^2}{c_-^4}$.

With equation (2.38) we can write down the inverse acoustic metric

$$g^{\mu\nu} = \frac{1}{n_0 c_-} \begin{pmatrix} -1 & -v^j \\ -v^i & c_-^2 \delta^{ij} - v^i v^j \end{pmatrix}, \tag{2.47}$$

and the metric itself

$$g_{\mu\nu} = \frac{n_0}{c_-} \begin{pmatrix} -\left(c_-^2 - v^2\right) & -v^j \\ -v^j & \delta^{ij} \end{pmatrix}. \tag{2.48}$$

The acoustic line element in the anti-symmetric degrees of freedom can be expressed as

$$ds^2 = \frac{n_0}{c_-} \left[-c_-^2 dt^2 + \left(dx^i - v^i dt\right) \delta_{ij} \left(dx^j - v^j dt\right)\right]. \tag{2.49}$$

In summary we expressed the equation of motion for the phase fluctuations in our two-

component condensate in terms of a Klein-Gordon equation for a massless (in the symmetric regime and in the anti-symmetric regime with $J = 0$) or massive (in the anti-symmetric regime with $J \neq 0$) scalar field propagating in a space-time described by the metric $g_{\mu\nu}$. This is the basic principle of analogue gravity!
However it is important to notice, that this analogue model is actually restricted to the hydrodynamic approximation, that is to long wavelength sound modes.

2.3 Quantum fluctuations around a black hole horizon in a two-component Bose Einstein condensate

2.3.1 Step-like background configuration

If the flow of a fluid contains a transition from an subsonic ($v < c$) upstream region (u) to a supersonic ($v > c$) downstream region (d), the point where the flow becomes supersonic behaves as an event horizon for sound waves [40]. We chose a setting where such a horizon only appears in the anti-symmetric degrees of freedom, while in the symmetric degrees of freedom the flow remains subsonic everywhere. By setting $\alpha(x) = \alpha_u \Theta(-x) + \alpha_d \Theta(x)$ and $J(x) = J_u \Theta(-x) + J_d \Theta(x)$, where Θ is the Heavy-side step function, we achieve a step-like structure with a possible horizon at $x = 0$. This gives us a configuration with a uniform density $n_{u,d} = n_0$ and velocity $v_{u,d} = v$ throughout the whole system which satisfies the continuity equation (2.9). If we now choose for example $\alpha_{u,d}$ and $J_{u,d}$ such that

$$c_{-,d} < v < c_{-,u} < c_{+,u} < c_{+,d}, \tag{2.50}$$

we obtain a horizon in the anti-symmetric regime and an everywhere subsonic flow in the symmetric regime. Of course it is also possible to find a configuration, where $c_{+,d} < c_{+,u}$ ($\alpha_u > \alpha_d > 1$ and $J_{u,d} \neq 0$) or where there is also a horizon in the symmetric degrees of freedom (just choose α_u, J_u and v such that $c_{+,u} < c_{-,u}$). Also a configuration with an horizon only in the symmetric regime, while the anti-symmetric is completely supersonic or subsonic (set $c_{+,u} < v < c_{+,d}$ and choose $J_{u,d}$ accordingly) is thinkable. Though most of this configurations are only realisable for $\omega_0 \neq 0$.
For now we will restrict ourselves to a configuration with a horizon in the anti-symmetric regime, $c_{-,d} < v < c_{-,u}$, and an everywhere subsonic flow in the symmetric-regime, $v < c_{+,u}, c_{+,d}$.

2.3.2 Dispersion relations and the different k-roots

In the first section of this chapter we derived the dispersion relations for our condensates, (2.16). As expected, the gapless dispersion relation is linear for small k, ($k\xi \ll 1$), and approaches the quadratic dispersion of single particles for large k, ($k\xi \gg 1$). Strictly speaking the gravitational analogy is only valid in the linear regime.

Since equations (2.16) are both fourth order polynomials, there are four k-roots for any $\omega > 0$. In the case of a subsonic background flow or no background flow at all and a gapless dispersion relation there are two real roots $k_{r|\mathrm{in}}$ and $k_{r|\mathrm{out}}$ with $r \in \{u, d\}$ having a positive norm and corresponding to propagating plane waves. The other two roots are complex conjugates to each other and have negative norm. They correspond to exponentially growing or decreasing evanescent waves. If the dispersion relation features a gap, there exists a ω^* such that for any $0 < \omega < \omega^*$ there are two pairs of complex conjugate k-roots, while for $\omega > \omega^*$ there are again the two real roots $k_{r|\mathrm{in}}$ and $k_{r|\mathrm{out}}$ and the pair of complex conjugates.
In figure 2.1 we plotted the dispersion relation (2.16b) for a subsonic flow in the anti-symmetric regime with (lower panel) and without (upper panel) a gap. The red dots, labelled as $u|$in and $u|$out, indicate the two real roots $k_{u|\mathrm{in}}$ and $k_{u|\mathrm{out}}$. Throughout the whole thesis a mode labelled as "in" or "out" has a group velocity v_g pointing towards the horizon or away from it respectively. The darkorange dot labelled ω^* indicates the minimum frequency below which only complex k-roots exist.
One should notice, that the dispersion relations (2.16a) in the symmetric regime would look just like the one plotted in the upper panel of figure 2.1. However in the subsonic downstream region one has to relabel the $u|$out-mode as $d|$in and the $u|$in-mode as $d|$out respectively.
In any regime, the symmetric as well as the anti-symmetric, one should discard the wavevectors corresponding to evanescent modes with $\mathrm{Im}\,(k_\ell) > 0$ in the upstream region and the ones with $\mathrm{Im}\,(k_\ell) < 0$ in the downstream region, since they diverge for $x \to -\infty$ and $x \to \infty$ respectively. The remaining complex modes will be labelled $k_{r|\mathrm{eva}}$ with $r \in \{u, d\}$ for a gapless dispersion relation and $r \in \{u1, u2, d1, d2\}$ for a gaped one where $u1, d1$ indicate positive norm modes and $u2, d2$ negative norm modes.

In the case of a supersonic background flow and a gapless dispersion relation there exists a Ω^* such that for any $0 < \omega < \Omega^*$ there are four real root. Two of them, $k_{r1|\mathrm{in}}$ and $k_{r1|\mathrm{out}}$ belonging to the positive norm branch and the other two, $k_{r2|\mathrm{in}}$ and $k_{r2|\mathrm{out}}$ belonging

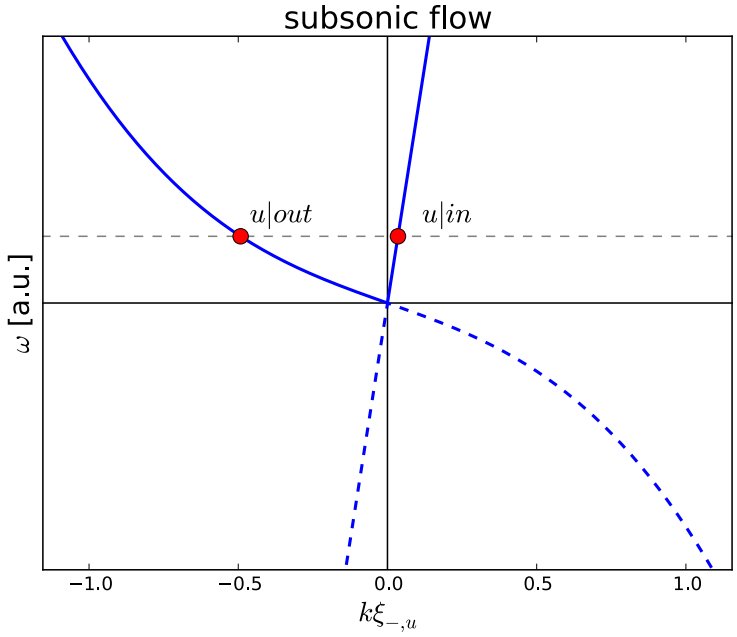

(a)

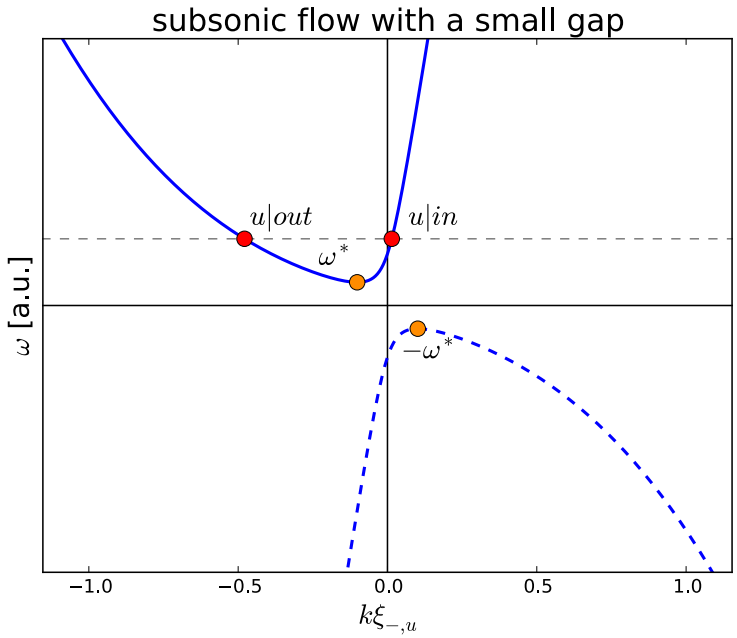

(b)

Figure 2.1: The Bogoliubov dispersion relation (2.16b) for the subsonic upstream region of the anti-symmetric degrees of freedom without (upper panel) and with (lower panel) gap. The positive norm branch is represented by a solid line, the negative norm branch by a dashed line. Red dots indicate the two real eigenmodes for a fixed ω. Darkorange dots indicate the minimum frequency ω^* for which real k-roots still exist.

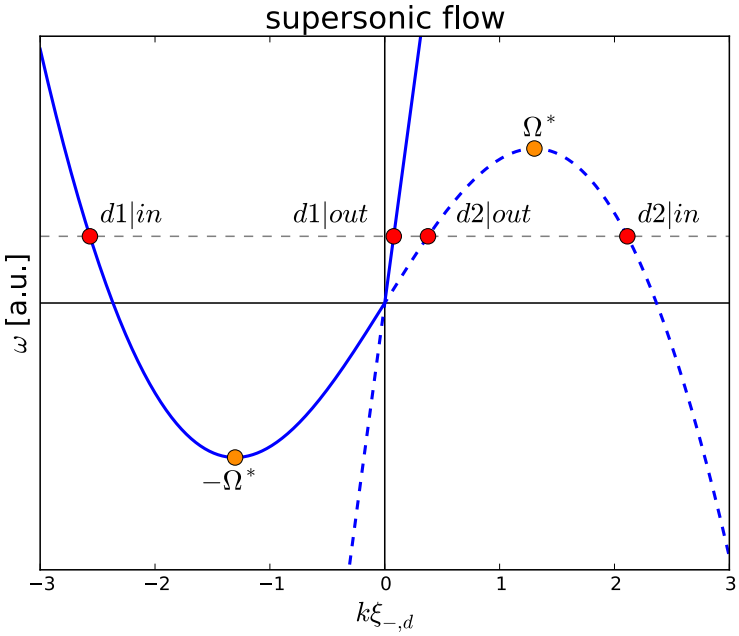

(a)

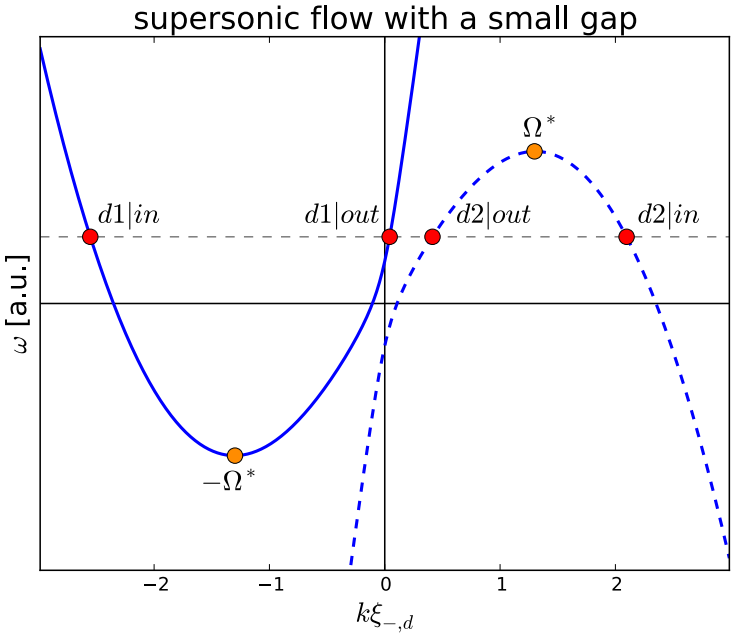

(b)

Figure 2.2: The Bogoliubov dispersion relation (2.16b) for the supersonic downstream region of the anti-symmetric degrees of freedom without (upper panel) and with (lower panel) gap. The positive norm branches are represonted by a solid line, the negative norm branches by a dashed line. Red dots indicate the four real eigenmodes for a fixed ω, darkorange dots the maximum (minimum) frequency Ω^* below (above) which all four eigenmodes are real.

to the negative norm branch. For any $\omega > \Omega^*$ there are again two real roots $k_{r1|\mathrm{in}}$ and $k_{r1|\mathrm{out}}$, and two complex ones of which one has to be discarded. The dispersion relation for the anti-symmetric degrees of freedom is plotted in the upper panel of figure 2.2. Again, if we had a supersonic flow in the symmetric regime, the dispersion relation would look just like the plotted one.
In the presence of a gap there are two possible cases. For a small gap, as plotted in the lower panel of figure 2.2 the situation would be the same as in a gapless dispersion relation. However for a large gap, it is quite different. In this case the dispersion relation would look more like the one plotted in the lower panel of figure 2.1, which means there exists an $-\Omega^* > 0$ such that for any $0 < \omega < -\Omega^*$ all four k-roots are complex and for any $\omega > -\Omega^*$ two real and to complex k-roots exist.

2.3.3 Matching conditions at the horizon

In our step-like configuration the condensates are homogeneous on both sides of the horizon and the corresponding eigenmodes are well known to us, (2.26)-(2.29). However, these eigenmodes are restricted to the upstream or downstream region of our system and the true eigenmodes of the whole system are linear combinations of the channels in the upstream and downstream regions with appropriate matching at the horizon at $x = 0$. These matching conditions can be obtained by integrating the equations of motion (2.19) about an infinitesimal interval around the horizon, [43]. This results in the following generally valid conditions

$$\left[\delta\tilde{\theta}_a\right]_{x\to 0^\pm} = 0, \tag{2.51a}$$

$$\left[v\delta\tilde{n}_a + \lambda_a \frac{1}{m}\partial_x \delta\tilde{\theta}_a\right]_{x\to 0^\pm} = 0, \tag{2.51b}$$

$$\left[\delta\tilde{n}_a\right]_{x\to 0^\pm} = 0, \tag{2.51c}$$

$$\left[\frac{1}{\lambda_a}\frac{1}{2m}\partial_x \delta\tilde{n}_a - v\delta\tilde{\theta}_a\right]_{x\to 0^\pm} = 0, \tag{2.51d}$$

where the square brackets on the left side denote $[*]_{x\to 0^\pm} = *|_{x\to 0^+} - *|_{x\to 0^-}$.
Since we chose our background flow to have constant velocity v everywhere, the above

matching conditions simplify to

$$\left[\delta\tilde{\theta}_a\right] = 0, \tag{2.52a}$$
$$\left[\partial_x \delta\tilde{\theta}_a\right] = 0, \tag{2.52b}$$
$$\left[\delta\tilde{n}_a\right] = 0, \tag{2.52c}$$
$$\left[\partial_x \delta\tilde{n}_a\right] = 0. \tag{2.52d}$$

By use of the quantisation (2.21) and defining

$$\Pi_{a,r}(x) = \begin{pmatrix} f^+_{a,r}(x) \\ f^-_{a,r}(x) \end{pmatrix}, \tag{2.53}$$

and

$$\varpi_{a,\ell}(x) = e^{ik_\ell x} \begin{pmatrix} F^+_{a,\ell}(x) \\ F^-_{a,\ell}(x) \end{pmatrix}, \tag{2.54}$$

the matching conditions can be rewritten for the modefunctions

$$\left[\Pi_{a,r}\right] = 0, \tag{2.55a}$$
$$\left[\partial_x \Pi_{a,r}\right] = 0. \tag{2.55b}$$

Here the index r indicates which side of the horizon is considered and is therefore equal to either u or d. The index ℓ labels the eigenmodes of equation (2.24), that is for instance for a gapless configuration in the anti-symmetric degrees of freedom $\ell \in \{u|\text{in}, u|\text{out}, u|\text{eva}, d1|\text{in}, d1|\text{out}, d2|\text{in}, d2|\text{out}, d|\text{eva}\}$. So more precisely that means $\Pi_{a,u}$ describes the excitations in the subsonic region and is a linear combination of $\varpi_{a,u|\text{in}}$, $\varpi_{a,u|\text{out}}$ and $\varpi_{a,u|\text{eva}}$.

2.3.4 The scattering solution

Among all the possible combinations described in the above section 2.3.3, the most remarkable ones are the scattering modes. These are modes originating from infinity (either upstream or downstream) on a well defined ingoing mode, impinging on the

horizon, and leaving again towards infinity as a superposition of the transmitted and reflected outgoing modes.
It is intuitive to label these scattering modes according to their incoming channels u, d in the symmetric regime and $u, d1, d2$ for the anti-symmetric regime. However, we already used these to label the individual ingoing and outgoing modes. Therefore, to avoid confusion, we will use capital letters and denote the scattering modes as Π_+^U and Π_+^D in the symmetric regime and Π_-^U, Π_-^{D1} and Π_-^{D2} in the anti-symmetric regime. Since all these modes have different analytic expressions on each side of the horizon we will additionally label them with u and d for upstream and downstream respectively.
In the following we will specify the expression for each of the scattering modes. Thereto we consider the symmetric and anti-symmetric degrees of freedom separately, since, as indicated by the decoupled equations of motion (2.19) and shown in [31, 32], an ingoing mode in the symmetric (anti-symmetric) regime does not scatter into any outgoing mode in the anti-symmetric (symmetric) regime.

We will first give the expressions of the scattering modes in the symmetric regime for an overall subsonic flow. It is worth noticing that the following modes are the only possible scattering modes as long as the flow remains subsonic.
For legibility, we did not display the x-dependence of the individual mode vectors Π and ϖ in the following.

U mode, initiated by $u|\text{in}$ in the symmetric regime

$$\Pi^U_{+,u} = \varpi_{+,u|\text{in}} + S^+_{u,u}\varpi_{+,u|\text{out}} + S^{+,\text{eva}}_{u,u}\varpi_{+,u|\text{eva}}, \tag{2.56a}$$
$$\Pi^U_{+,d} = S^+_{d,u}\varpi_{+,d|\text{out}} + S^{+,\text{eva}}_{d,u}\varpi_{+,d|\text{eva}}. \tag{2.56b}$$

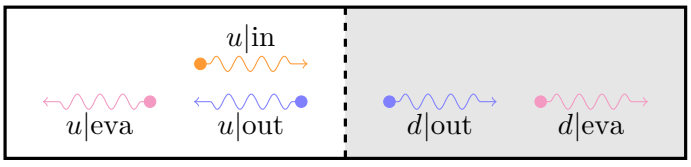

Figure 2.3: U mode, initiated by $u|\text{in}$ in the symmetric regime.

D mode, initiated by $d|\text{in}$ in the symmetric regime

$$\Pi^{D}_{+,u} = S^{+}_{u,d}\varpi_{+,u|\text{out}} + S^{+,\text{eva}}_{u,d}\varpi_{+,u|\text{eva}}, \tag{2.57a}$$

$$\Pi^{D}_{+,d} = \varpi_{+,d|\text{in}} + S^{+}_{d,d}\varpi_{+,d|\text{out}} + S^{+,\text{eva}}_{d,d}\varpi_{+,d|\text{eva}}. \tag{2.57b}$$

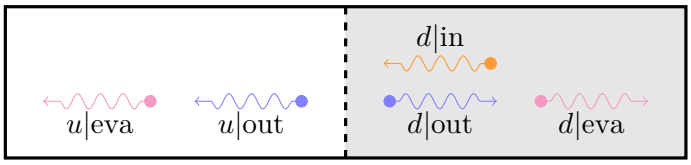

Figure 2.4: D mode, initiated by $d|\text{in}$ in the symmetric regime.

In figures 2.3, 2.4 the two different scattering modes are displayed in a pictorial way. In contrast to figure 2.1a where the evanescent modes cannot be represented, here they are depicted as magenta wiggles.
The scattering coefficients, $S^{+}_{u,u}, S^{+,\text{eva}}_{u,u}, S^{+}_{d,u}$, etc. are determined by solving the two (4×4) systems of linear equations (2.55). They are independent of x but depend on ω. Their square moduli $\left|S^{+}_{\ell,\ell'}(\omega)\right|^2$ give the transmission or reflection coefficient for an ℓ-ingoing mode at energy $\hbar\omega$ into an ℓ'-outgoing mode at the same energy.
To ensure total energy conservation the S matrix

$$\mathbf{S}^{+}(\omega) = \begin{pmatrix} S^{+}_{u,u} & S^{+}_{u,d} \\ S^{+}_{d,u} & S^{+}_{d,d} \end{pmatrix}, \tag{2.58}$$

is unitary and therefore has to fulfil the unitarity condition $\mathbf{S}^{+}(\mathbf{S}^{+})^{\dagger} = \mathbb{1} = (\mathbf{S}^{+})^{\dagger}\mathbf{S}^{+}$. The scattering coefficients corresponding to evanescent modes are not involved in energy current conservation since the evanescent waves carry no current.

In figure 2.5 we plotted the scattering coefficients as a function of the frequency ω_{+}. As expected, the transmission coefficients $\left|S^{+}_{u,d}\right|^2$ and $\left|S^{+}_{d,u}\right|^2$ increase while the reflection coefficients $\left|S^{+}_{u,u}\right|^2$ and $\left|S^{+}_{d,d}\right|^2$ decrease with ω_{+}. The unitarity condition of the scattering matrix imposes that the sum of these two coefficicents is always equal to unity. The errors in our numeric calculations are smaller than 10^{-7}.

We will now continue to give the expressions of the scattering modes in the anti-symmetric regime with an subsonic upstream region and a supersonic downstream region.

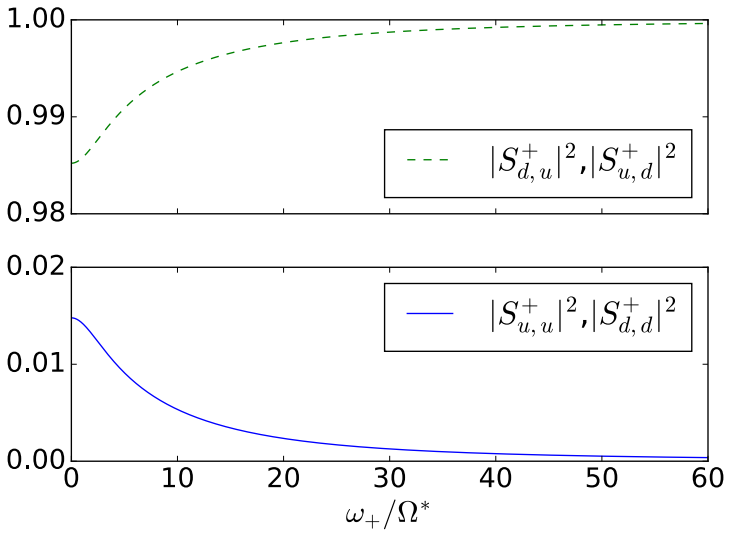

Figure 2.5: Transmission and reflection coefficient for the symmetric degrees of freedom. We used the parameters $\alpha_u = 0.2$, $J_{u,d} = 0$, $v/c_{-,u} = 0.7$ and $v/c_{-,d} = 3$. This gives us $v/c_{+,u} = 0.572$ and $v/c_{+,d} = 0.448$ in the symmetric regime. $\left|S^+_{d,u}\right|^2$ $\left(\left|S^+_{u,d}\right|^2\right)$ corresponds to the transmission of a u-ingoing (d-ingoing) mode to a d-outgoing (u-outgoing) mode. $\left|S^+_{u,u}\right|^2$ $\left(\left|S^+_{d,d}\right|^2\right)$ corresponds to the reflection of a u-ingoing (d-ingoing) mode into a u-outgoing (d-outgoing) mode.

We assume a configuration with a gapless dispersion relation.

U mode, initiated by $u|\text{in}$ in the anti-symmetric regime

$$\Pi^U_{-,u} = \varpi_{-,u|\text{in}} + S^-_{u,u}\varpi_{-,u|\text{out}} + S^{-,\text{eva}}_{u,u}\varpi_{-,u|\text{eva}}, \tag{2.59a}$$

$$\Pi^U_{-,d} = S^-_{d1,u}\varpi_{-,d1|\text{out}} + \Theta\left(\Omega^* - \omega\right) S^-_{d2,u}\varpi_{-,d2|\text{out}} + \Theta\left(\omega - \Omega^*\right) S^{-,\text{eva}}_{d,u}\varpi_{+,d|\text{eva}}. \tag{2.59b}$$

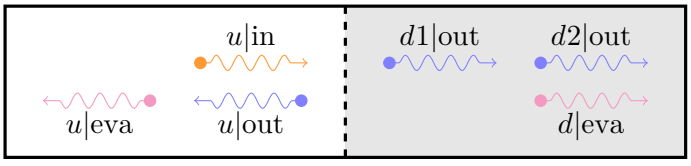

Figure 2.6: U mode, initiated by $u|\text{in}$ in the anti-symmetric regime.

$D1$ mode, initiated by $d1|\text{in}$ in the anti-symmetric regime

$$\Pi^{D1}_{-,u} = S^{-}_{u,d1}\varpi_{-,u|\text{out}} + S^{-,\text{eva}}_{u,d1}\varpi_{-,u|\text{eva}}, \tag{2.60a}$$

$$\Pi^{D1}_{-,d} = \varpi_{-,d1|\text{in}} + S^{-}_{d1,d1}\varpi_{-,d1|\text{out}} + \Theta\left(\Omega^* - \omega\right) S^{-}_{d2,d1}\varpi_{-,d2|\text{out}} + \Theta\left(\omega - \Omega^*\right) S^{-,\text{eva}}_{d,d1}\varpi_{+,d|\text{eva}}. \tag{2.60b}$$

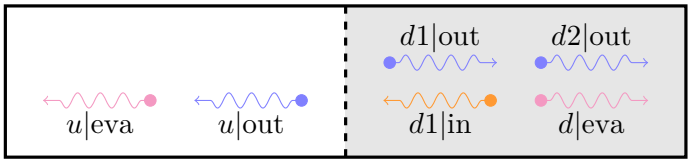

Figure 2.7: $D1$ mode, initiated by $d1|\text{in}$ in the anti-symmetric regime.

$D2$ mode, initiated by $d2|\text{in}$ in the anti-symmetric regime

$$\Pi^{D2}_{-,u} = \Theta\left(\Omega^* - \omega\right)\left[S^{-}_{u,d2}\varpi_{-,u|\text{out}} + S^{-,\text{eva}}_{u,d2}\varpi_{-,u|\text{eva}}\right], \tag{2.61a}$$

$$\Pi^{D2}_{-,d} = \Theta\left(\Omega^* - \omega\right)\left[\varpi_{-,d2|\text{in}} + S^{-}_{d1,d2}\varpi_{-,d1|\text{out}} + S^{-}_{d2,d2}\varpi_{-,d2|\text{out}}\right]. \tag{2.61b}$$

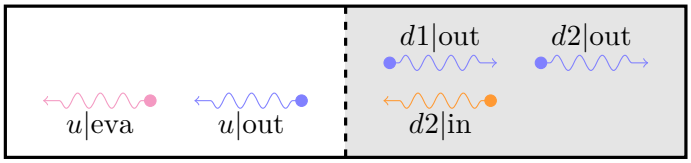

Figure 2.8: $D2$ mode, initiated by $d2|\text{in}$ in the anti-symmetric regime.

As before, the three different scattering modes are displayed in a pictorial way in figures 2.6-2.8, where the evanescent modes are again depicted as magenta wiggles. Note that for $\omega < \Omega^*$ the evanescent mode inside the black hole is replaced by the $d2$-outgoing mode. Also the $D2$ scattering mode only exists for $\omega < \Omega^*$. For $\omega > \Omega^*$ there are only two scattering modes. This is taken care of in formulas (2.59)-(2.61) by the Heaviside step functions $\Theta\left(\Omega^* - \omega\right)$ and $\Theta\left(\omega - \Omega^*\right)$.
For $\omega > \Omega^*$ the S matrix is again a 2×2 unitary matrix, just as in (2.58). However for $\omega < \Omega^*$ the downstream evanescent mode has to be replaced by the $d2|\text{out}$ mode and the S matrix is a 3×3 matrix

$$\mathbf{S}^{-}(\omega) = \begin{pmatrix} S^{-}_{u,u} & S^{-}_{u,d1} & S^{-}_{u,d2} \\ S^{-}_{d1,u} & S^{-}_{d1,d1} & S^{-}_{d1,d2} \\ S^{-}_{d2,u} & S^{-}_{d2,d1} & S^{-}_{d2,d2} \end{pmatrix}, \tag{2.62}$$

with a skew unitarity imposing the condition

$$(\mathbf{S}^{-})^{\dagger}\,\eta\mathbf{S}^{-} = \eta = \mathbf{S}^{-}\eta\,(\mathbf{S}^{-})^{\dagger}\,, \tag{2.63}$$

with a Bogoliubov metric $\eta = \mathrm{diag}\,(1, 1, -1)$ inherited by the norm of the corresponding plane-wave modes.

In figure 2.9 we again plotted the scattering coefficients as a function of the frequency $\omega_{\_}$. For $\omega_{\_} > \Omega^{*}$ the reflection coefficients $\left|S^{-}_{u,u}\right|^{2}$ and $\left|S^{-}_{d1,d1}\right|^{2}$ and the transmission coefficients $\left|S^{-}_{d1,u}\right|^{2}$ and $\left|S^{-}_{u,d1}\right|^{2}$ recover the usual behaviour expected in wave mechanics, they decrease and increase respectively with the frequency $\omega_{\_}$. Scattering coefficients containing an $d2$-ingoing or $d2$-outgoing mode do not exist for $\omega_{\_} > \Omega^{*}$ since the negative norm $d2$-ingoing and $d2$-outgoing modes are only involved in the dynamics for $\omega_{\_} < \Omega^{*}$. Remarkably, all the coefficients of the form $\left|S^{-}_{i,d1}\right|^{2}$ and $\left|S^{-}_{i,d2}\right|^{2}$ diverge at low $\omega_{\_}$. This is a signature of the occurrence of an event horizon for the low energy modes. Low energy quasiparticles entering the system from the interior of the dump hole, that is through the $d1|$in or $d2|$out channel, remain blocked at the horizon forever. Despite the diverging scattering coefficients energy conservation is still ensured by the skew unitarity of the scattering matrix.
Here too the errors in our numeric calculations are smaller than 10^{-7}.

As shown in [31, 32, 26, 28] the scattering coefficients can by calculated analytically in the low ω limit.

Last we consider the scattering modes for the anti-symmetric degrees of freedom in the presence of a horizon and a small gap in the dispersion relation. As we saw in figure 2.1b there now exists an ω^{*} such that for any $0 < \omega < \omega^{*}$ the outgoing mode in the upstream region is replaced by a second evanescent mode. Also the U scattering mode only exist for $\omega > \omega^{*}$.
The explicit expressions of the scattering modes are given below.

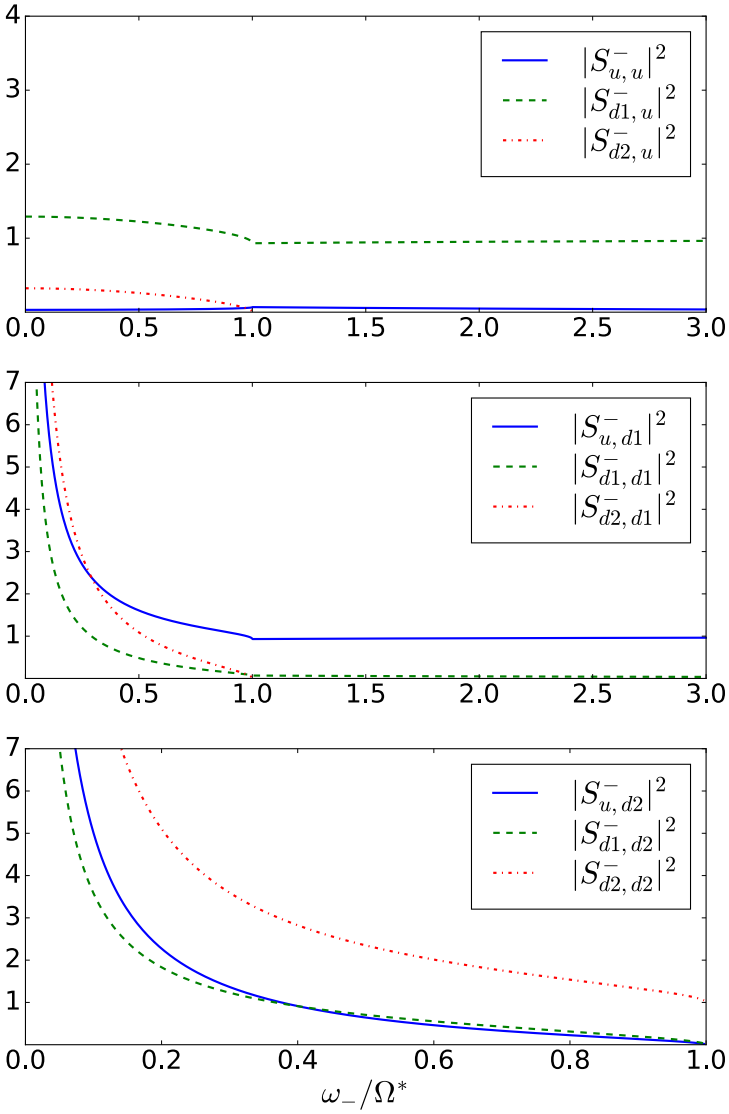

Figure 2.9: Transmission and reflection coefficient for a u-ingoing mode (upper panel), a $d1$-ingoing mode (middle panel) and a $d2$-ingoing mode (lower panel) on a step-like dumb hole configuration for the anti-symmetric degrees of freedom. We used the parameters $\alpha_u = 0.2$, $J_{u,d} = 0$, $v/c_{-,u} = 0.7$ and $v/c_{-,d} = 3$. Coefficients involving a $d2$-ingoing or a $d2$-outgoing mode only exist for $\omega_- < \Omega^*$.

U mode, initiated by $u|\text{in}$ in the anti-symmetric regime

$$\Pi^{U}_{-,u} = \Theta\left(\omega-\omega^{*}\right)\left[\varpi_{-,u1|\text{in}} + S^{-}_{u1,u1}\varpi_{-,u1|\text{out}} + S^{-,\text{eva}}_{u2,u1}\varpi_{-,u2|\text{eva}}\right], \tag{2.64a}$$

$$\begin{aligned}\Pi^{U}_{-,d} = {}& \Theta\left(\omega-\omega^{*}\right)\left[S^{-}_{d1,u1}\varpi_{-,d1|\text{out}} + \Theta\left(\Omega^{*}-\omega\right)S^{-}_{d2,u1}\varpi_{-,d2|\text{out}}\right.\\ & \left. + \Theta\left(\omega-\Omega^{*}\right)S^{-,\text{eva}}_{d,u1}\varpi_{+,d|\text{eva}}\right].\end{aligned} \tag{2.64b}$$

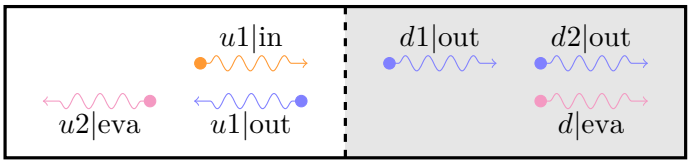

Figure 2.10: U mode, initiated by $u|\text{in}$ in the anti-symmetric regime with a gaped dispersion relation.

$D1$ mode, initiated by $d1|\text{in}$ in the anti-symmetric regime

$$\begin{aligned}\Pi^{D1}_{-,u} = {}& \Theta\left(\omega-\omega^{*}\right)S^{-}_{u1,d1}\varpi_{-,u|\text{out}}\\ & + \Theta\left(\omega^{*}-\omega\right)S^{-,\text{eva}}_{u1,d1}\varpi_{-,u1|\text{eva}} + S^{-,\text{eva}}_{u2,d1}\varpi_{-,u2|\text{eva}},\end{aligned} \tag{2.65a}$$

$$\begin{aligned}\Pi^{D1}_{-,d} = {}& \varpi_{-,d1|\text{in}} + S^{-}_{d1,d1}\varpi_{-,d1|\text{out}} + \Theta\left(\Omega^{*}-\omega\right)S^{-}_{d2,d1}\varpi_{-,d2|\text{out}}\\ & + \Theta\left(\omega-\Omega^{*}\right)S^{-,\text{eva}}_{d,d1}\varpi_{+,d|\text{eva}}.\end{aligned} \tag{2.65b}$$

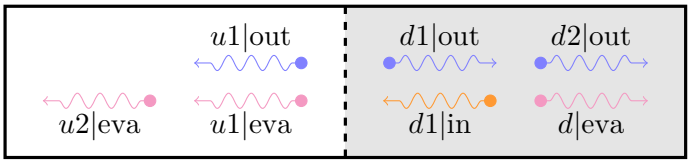

Figure 2.11: $D1$ mode, initiated by $d1|\text{in}$ in the anti-symmetric regime with a gaped dispersion relation.

$D2$ mode, initiated by $d2|\text{in}$ in the anti-symmetric regime

$$\begin{aligned}\Pi^{D2}_{-,u} = {}& \Theta\left(\Omega^{*}-\omega\right)\left[\Theta\left(\omega-\omega^{*}\right)S^{-}_{u1,d2}\varpi_{-,u1|\text{out}}\right.\\ & \left. + \Theta\left(\omega^{*}-\omega\right)S^{-,\text{eva}}_{u1,d2}\varpi_{-,u1|\text{eva}} + S^{-,\text{eva}}_{u2,d2}\varpi_{-,u2|\text{eva}}\right],\end{aligned} \tag{2.66a}$$

$$\Pi^{D2}_{-,d} = \Theta\left(\Omega^{*}-\omega\right)\left[\varpi_{-,d2|\text{in}} + S^{-}_{d1,d2}\varpi_{-,d1|\text{out}} + S^{-}_{d2,d2}\varpi_{-,d2|\text{out}}\right]. \tag{2.66b}$$

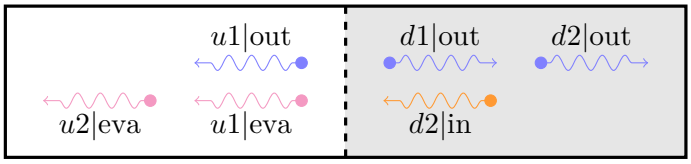

Figure 2.12: $D2$ mode, initiated by $d2|\text{in}$ in the anti-symmetric regime with a gaped dispersion relation.

Now, for $\omega > \omega^*, \Omega^*$ the scattering matrix is again an 2×2 unitary matrix as in (2.58) satisfying the usual unitarity conditions. For $\omega^* < \omega < \Omega^*$ the scattering matrix becomes a 3×3 matrix as in (2.62) with a skew unitarity condition as in (2.63). For $\omega < \omega^*, \Omega^*$ the scattering matrix is again a 2×2 matrix

$$\mathbf{S}^{-}(\omega) = \begin{pmatrix} S^{-}_{d1,d1} & S^{-}_{d1,d2} \\ S^{-}_{d2,d1} & S^{-}_{d2,d2} \end{pmatrix} \tag{2.67}$$

though still with a skew unitarity imposing the condition (2.63) with a different metric $\eta = \text{diag}(1, -1)$, again inherited by the norm of the corresponding plane-wave modes. In the case of $\Omega^* < \omega < \omega^*$ only the $D1$ scattering mode would still exist and therefore the scattering matrix would be reduced to $S^{-}_{d1,d1}$. That means the $d1$ ingoing mode would be completely reflected into the $d1$ outgoing mode. We are not interested in such a configuration where no $d2$ modes exist anymore since the Hawking signal outside of the black hole, as we will see later, originates in the $d2$ ingoing mode. For the same reason we are also not interested in configurations with a dispersion relation with a large gap.

In figure 2.13 we plotted the scattering coefficients as a function of the frequency $\omega_{\_}$. Again for $\omega_{\_} > \Omega^*$ the reflection coefficients $\left|S^{-}_{u,u}\right|^2$ and $\left|S^{-}_{d1,d1}\right|^2$ and the transmission coefficients $\left|S^{-}_{d1,u}\right|^2$ and $\left|S^{-}_{u,d1}\right|^2$ recover the usual behaviour expected in wave mechanics, they decrease and increase respectively with the frequency $\omega_{\_}$. Contrary to the case with $J_{u,d} = 0$, see figure 2.9, scattering coefficients containing an u-ingoing or u-outgoing mode only exist for $\omega_{\_} > \omega^*$. This is because in a gaped dispersion relation there are only evanescent modes in the upstream region for $\omega_{\_} < \omega^*$. Still coefficients of the form $\left|S^{-}_{i,d1}\right|^2$ and $\left|S^{-}_{i,d2}\right|^2$ with $i \in \{d1, d2\}$ diverge at low $\omega_{\_}$, again being a signature of the occurrence of an event horizon for the low energy modes. Though this time we are actually considering quasiparticles with an effective mass. So for any $\omega_{\_} < \omega^*$ quasiparticles entering the system from the interior of the black hole, that is through the $d1|\text{in}$ or $d2|\text{out}$ channel, are completely blocked at the horizon forever. Here again

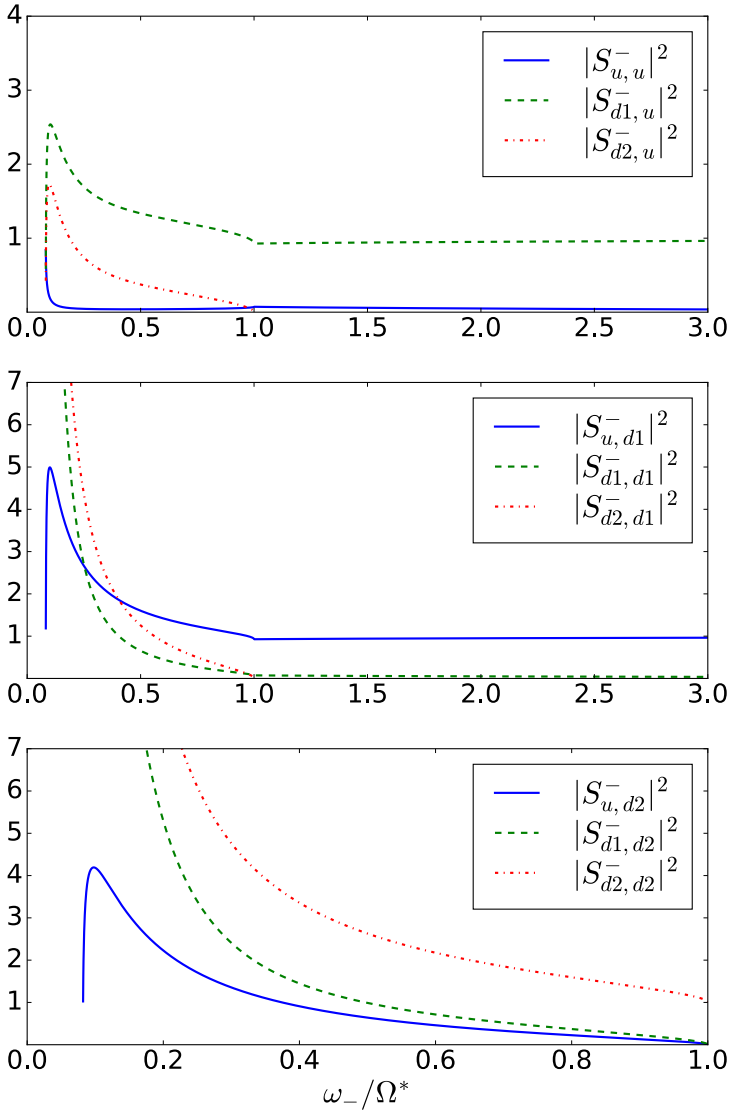

Figure 2.13: Transmission and reflection coefficient for a u-ingoing mode (upper panel), a $d1$-ingoing mode (middle panel) and a $d2$-ingoing mode (lower panel) on a step-like dumb hole configuration for the anti-symmetric degrees of freedom with a gaped dispersion relation. We used the parameters $\alpha_u = 0.2$, $J_u/n_0 g = 0,0001$, $v/c_{-,u} = 0.7$, $v/c_{-,d} = 3$ and $J\left(n_0 g\left(1-\alpha\right)+J\right) = const.$. Coefficients involving a $d2$-ingoing or a $d2$-outgoing mode only exist for $\omega_- < \Omega^*$ while coefficients involving a u-ingoing or a u-outgoing mode only exist for $\omega_- > \omega^*$.

energy conservation is ensured by the skew unitarity of the scattering matrix.
Here too the errors in our numeric calculations are smaller than 10^{-7}.

2.3.5 Quantisation

We now expand the field operators $\delta\tilde{n}_a$ and $\delta\tilde{\theta}_a$ ($a \in \{+,-\}$) associated (in the Heisenberg representation) to the elementary excitations over the scattering modes.
For the symmetric degrees of freedom, or any overall subsonic system, this expansion is

$$\begin{aligned}&\delta\tilde{n}_+(x,t) = \\ &\sqrt{2}\int_0^\infty \frac{d\omega}{\sqrt{2\pi}} \sum_{L\in\{U,D\}} \left[f^+_{+,L}(\omega,x)\, e^{-i\omega t}\hat{b}_L(\omega) + \left(f^+_{+,L}(\omega,x)\right)^* e^{i\omega t}\hat{b}^\dagger_L(\omega)\right],\end{aligned} \tag{2.68a}$$

$$\begin{aligned}&\delta\tilde{\theta}_+(x,t) = \\ &\frac{1}{i\sqrt{8}}\int_0^\infty \frac{d\omega}{\sqrt{2\pi}} \sum_{L\in\{U,D\}} \left[f^-_{+,L}(\omega,x)\, e^{-i\omega t}\hat{b}_L(\omega) - \left(f^-_{+,L}(\omega,x)\right)^* e^{i\omega t}\hat{b}^\dagger_L(\omega)\right],\end{aligned} \tag{2.68b}$$

while for the anti-symmetric degrees of freedom, or any system with a horizon, it is

$$\begin{aligned}&\delta\tilde{n}_-(x,t) = \\ &\sqrt{\frac{1}{2}}\int_0^\infty \frac{d\omega}{\sqrt{2\pi}} \sum_{L\in\{U,D1\}} \left[f^+_{-,L}(\omega,x)\, e^{-i\omega t}\hat{b}_L(\omega) + \left(f^+_{-,L}(\omega,x)\right)^* e^{i\omega t}\hat{b}^\dagger_L(\omega)\right] \\ &+\sqrt{\frac{1}{2}}\int_0^{\Omega^*} \frac{d\omega}{\sqrt{2\pi}} \left[f^+_{-,D2}(\omega,x)\, e^{-i\omega t}\hat{b}^\dagger_{D2}(\omega) + \left(f^+_{-,D2}(\omega,x)\right)^* e^{i\omega t}\hat{b}_{D2}(\omega)\right],\end{aligned} \tag{2.69a}$$

$$\begin{aligned}&\delta\tilde{\theta}_-(x,t) = \\ &\frac{1}{i\sqrt{2}}\int_0^\infty \frac{d\omega}{\sqrt{2\pi}} \sum_{L\in\{U,D1\}} \left[f^-_{-,L}(\omega,x)\, e^{-i\omega t}\hat{b}_L(\omega) - \left(f^-_{-,L}(\omega,x)\right)^* e^{i\omega t}\hat{b}^\dagger_L(\omega)\right] \\ &+\frac{1}{i\sqrt{2}}\int_0^{\Omega^*} \frac{d\omega}{\sqrt{2\pi}} \left[f^-_{-,D2}(\omega,x)\, e^{-i\omega t}\hat{b}^\dagger_{D2}(\omega) - \left(f^-_{-,D2}(\omega,x)\right)^* e^{i\omega t}\hat{b}_{D2}(\omega)\right],\end{aligned} \tag{2.69b}$$

Note that the cutoffs in the second integrals in (2.69a) and (2.69b) at Ω^* are due to the

Heaviside step functions in (2.61). In case of a gaped dispersion relation the integral starts at ω^*, which is due to the Heaviside step function in (2.64).
The operators $\hat{b}_L^\dagger(\omega)$ and $\hat{b}_L(\omega)$ are the creation and annihilation operators of an excitation of energy $\hbar\omega$ in one of three (two) scattering modes $U, D1$ and $D2$ (U and D) in the anti-symmetric (symmetric) regime. They obey the bosonic commutation relations

$$\left[\hat{b}_L(\omega), \hat{b}_{L'}^\dagger(\omega')\right] = \delta_{L,L'}\delta(\omega-\omega'), \tag{2.70a}$$

$$\left[\hat{b}_L^\dagger(\omega), \hat{b}_{L'}^\dagger(\omega')\right] = 0 = \left[\hat{b}_L(\omega), \hat{b}_{L'}(\omega')\right]. \tag{2.70b}$$

Also note that for the $D2$ scattering mode the role of the creation and annihilation operators is exchanged compared to the U and $D1$ scattering modes. That is a consequence of the negative Bogoliubov norm of the $d2$ ingoing mode, from which the $D2$ scattering mode originates.

3 Density correlations

As first remarked in [24] and adopted in later works [26, 28, 31, 32, 36], the two point density correlation function seems to be a highly promising tool for identifying acoustic Hawing radiation.
In a two-component Bose gas the 2-point density correlation function for the symmetric and anti-symmetric degrees of freedom is defined as

$$\begin{aligned} g_{\pm}^{(2)}(x_1, x_2) &= \langle :n_{\pm}(x_1, t)\, n_{\pm}(x_2, t): \rangle \\ &= \langle n_{\pm}(x_1, t)\, n_{\pm}(x_2, t) \rangle - \langle n_{+}(x_1, t) \rangle \delta(x_1 - x_2), \end{aligned} \tag{3.1}$$

where we defined

$$n_{\pm}(x, t) = \psi_1^{\dagger}(x, t)\, \psi_1(x, t) \pm \psi_2^{\dagger}(x, t)\, \psi_2(x, t). \tag{3.2}$$

Comparing (3.2) with the definitions (2.6) and (2.10) gives us

$$n_{+}(x, t) = 2n_0(x) + \sqrt{n_0(x)}\tilde{\delta n}_{+}, \tag{3.3a}$$

$$n_{-}(x, t) = 2\sqrt{n_0(x)}\tilde{\delta n}_{-}. \tag{3.3b}$$

3.1 Density correlations in the symmetric degrees of freedom

In the symmetric degrees of freedom the density correlation function $g_{+}^{(2)}(x_1, x_2)$ can be written as

$$g_{+}^{(2)}(x_1, x_2) = 4n_0^2 + n_0 \left\langle \tilde{\delta n}_{+}(x_1, t)\, \tilde{\delta n}_{+}(x_2, t) \right\rangle - 2n_0 \delta(x_1 - x_2), \tag{3.4}$$

where we used (3.3a). For convenience we drop the $4n_0^2$ term, which is just a constant, and only consider the correlations of the fluctuations.
With the decomposition (2.68a) equation (3.4) can be recast into

$$g_{+}^{(2)}(x_1,x_2) = 2n_0 \int_0^\infty \frac{d\omega}{2\pi} \gamma_{+}(x_1,x_2,\omega) - 2n_0 \delta(x_1 - x_2), \tag{3.5}$$

where it is convenient to split $\gamma_{+}(x_1,x_2,\omega)$ and therefore $g_{+}^{(2)}(x_1,x_2)$ into a zero-temperature term $\gamma_{+,0}(x_1,x_2,\omega)$ and a thermal one $\gamma_{+,\mathrm{th}}(x_1,x_2,\omega)$:

$$\gamma_{+}(x_1,x_2,\omega) = \gamma_{+,0}(x_1,x_2,\omega) + \gamma_{+,\mathrm{th}}(x_1,x_2,\omega). \tag{3.6}$$

$\gamma_{+,0}(x_1,x_2,\omega)$ and accordingly $g_{+,0}^{(2)}(x_1,x_2,\omega)$ only involves the zero-point fluctuations of the in-going modes and stays finite even in the $T=0$ case, where the occupation number $\mathcal{N}_L(\omega) = \left\langle \hat{b}_L^\dagger(\omega)\, \hat{b}_L(\omega) \right\rangle = 0$. The zero-temperature contribution is

$$\gamma_{+,0}(x_1,x_2,\omega) = \sum_{L\in\{U,D\}} f_{+,L}^{+}(x_1) \left(f_{+,L}^{+}(x_2)\right)^*. \tag{3.7}$$

The thermal contribution $\gamma_{+,\mathrm{th}}(x_1,x_2,\omega)$ and accordingly $g_{+,\mathrm{th}}^{(2)}(x_1,x_2,\omega)$ vanishes in the $T=0$ case since it includes the initial population $\mathcal{N}_L(\omega)$. It can be written as

$$\begin{aligned}\gamma_{+,\mathrm{th}}(x_1,x_2,\omega) = \sum_{L\in\{U,D\}} &\left[f_{+,L}^{+}(x_1)\left(f_{+,L}^{+}(x_2)\right)^* + \left(f_{+,L}^{+}(x_1)\right)^* f_{+,L}^{+}(x_2)\right] \times \\ &\times \left\langle \hat{b}_L^\dagger(\omega)\, \hat{b}_L(\omega) \right\rangle.\end{aligned} \tag{3.8}$$

In the following we will give the explicit expressions for $\gamma_{+,0}(x_1,x_2,\omega)$, though for simplicity, we will restrict ourselves to the case where x_1 and x_2 are far from the horizon. This allows us to neglect the evanescent contributions to (3.7).

1. Case: x_1 and x_2 are both deep in the upstream region, $x_1, x_2 \ll -\xi_{+,u}$

$$\begin{aligned}\gamma_{+,0}(x_1,x_2,\omega) = &\left|F_{+,u|\mathrm{in}}^{+}\right|^2 e^{ik_{u|\mathrm{in}}(x_1-x_2)} \\ &+ \left|F_{+,u|\mathrm{out}}^{+}\right|^2 e^{ik_{u|\mathrm{out}}(x_1-x_2)},\end{aligned} \tag{3.9}$$

where we used

$$\left|S_{u,u}^{+}\right|^2 + \left|S_{u,d}^{+}\right|^2 = 1, \tag{3.10}$$

which comes from the unitarity of the scattering matrix (2.58).

2. Case: x_1 is deep in the upstream region, x_2 deep in the downstream region, $x_1 \ll -\xi_{+,u}$ and $x_2 \gg \xi_{+,d}$

$$\gamma_{+,0}\left(x_1, x_2, \omega\right) = 0, \tag{3.11}$$

where we used

$$S^{+}_{u,u}\left(S^{+}_{d,u}\right)^{*} + S^{+}_{u,d}\left(S^{+}_{d,d}\right)^{*} = 0. \tag{3.12}$$

3. Case: x_1 is deep in the downstream region, x_2 deep in the upstream region, $x_1 \gg \xi_{+,d}$ and $x_2 \ll -\xi_{+,u}$

$$\gamma_{+,0}\left(x_1, x_2, \omega\right) = 0, \tag{3.13}$$

where we used

$$S^{+}_{d,u}\left(S^{+}_{u,u}\right)^{*} + S^{+}_{d,d}\left(S^{+}_{u,d}\right)^{*} = 0. \tag{3.14}$$

4. Case: x_1 and x_2 are both deep in the downstream region, $x_1, x_2 \gg \xi_{+,d}$

$$\begin{aligned}\gamma_{+,0}\left(x_1, x_2, \omega\right) = &\left|F^{+}_{+,d|\mathrm{in}}\right|^2 e^{ik_{d|\mathrm{in}}(x_1 - x_2)} \\ &+ \left|F^{+}_{+,d|\mathrm{out}}\right|^2 e^{ik_{d|\mathrm{out}}(x_1 - x_2)},\end{aligned} \tag{3.15}$$

where we used

$$\left|S^{+}_{d,u}\right|^2 + \left|S^{+}_{d,d}\right|^2 = 1. \tag{3.16}$$

Note that the above expressions for $\gamma_{+,0}\left(x_1, x_2, \omega\right)$ would also be valid in the anti-symmetric subsonic regime for a configuration with a gapless dispersion relation and in

absence of a horizon.

In the case of a smooth background configuration, that is no step, the $u|$in mode would correspond with the $d|$out mode and the $u|$out mode with the $d|$in mode respectively. In such a homogeneous configuration where α has a constant uniform value and $J = 0$, the zero temperature correlator (3.5) can be written as [31, 32]

$$g_{+}^{(2)}(x_1, x_2) = \frac{2n_0}{\xi_{+}} F\left(\frac{|x_1 - x_2|}{\xi_{+}}\right), \tag{3.17}$$

with

$$F(z) = -\frac{1}{\pi z}\int_0^{\infty} dt \frac{\sin(2tz)}{(1+t^2)^{3/2}}, \tag{3.18}$$

which is the expected correlation in a quasi-1D condensate [44]. Formula (3.17) is also true for a smooth background configuration with a subsonic flow in the anti-symmetric degrees of freedom with $\xi_{+} \to \xi_{-}$.

However, for a step-like background configuration like ours, we see that the precise shape of the correlator is affected, due to the fact that the value of the healing length $\xi_{+,u}$ in the upstream region differs from $\xi_{+,d}$ in the downstream region. In figure 3.1 we plotted the quantity $\xi_{-,u} g_{+}^{(2)}(x_1, x_2)/2n_0$ in a configuration with a black hole only occuring in the anti-symmetric regime, while the background flow stays subsonic in the symmetric regime. We set $\alpha_u = 0.2$, $J_{u,d} = 0$, $v/c_{-,u} = 0.7$ and $v/c_{-,d} = 3$, which is $v/c_{+,u} = 0.572$ and $v/c_{+,d} = 0.448$. The integration in (3.5) was performed numerically and was cut off at $80\Omega^*$ which corresponds to $8.968\mu_u$ and $5.816\mu_d$. The shaded area near the axis corresponds to the zone $|x_1|, |x_2| < 10\xi_{-,u}$, where our formulas are not valid. As expected, the correlator for the symmetric degrees of freedom is similar to the short-range antibunching of a homogeneous configuration and shows no sign of the Hawking signal.

3.2 Density correlations in the anti-symmetric degrees of freedom

In the anti-symmetric degrees of freedom the density correlation function $g_{-}^{(2)}(x_1, x_2)$ can be written as

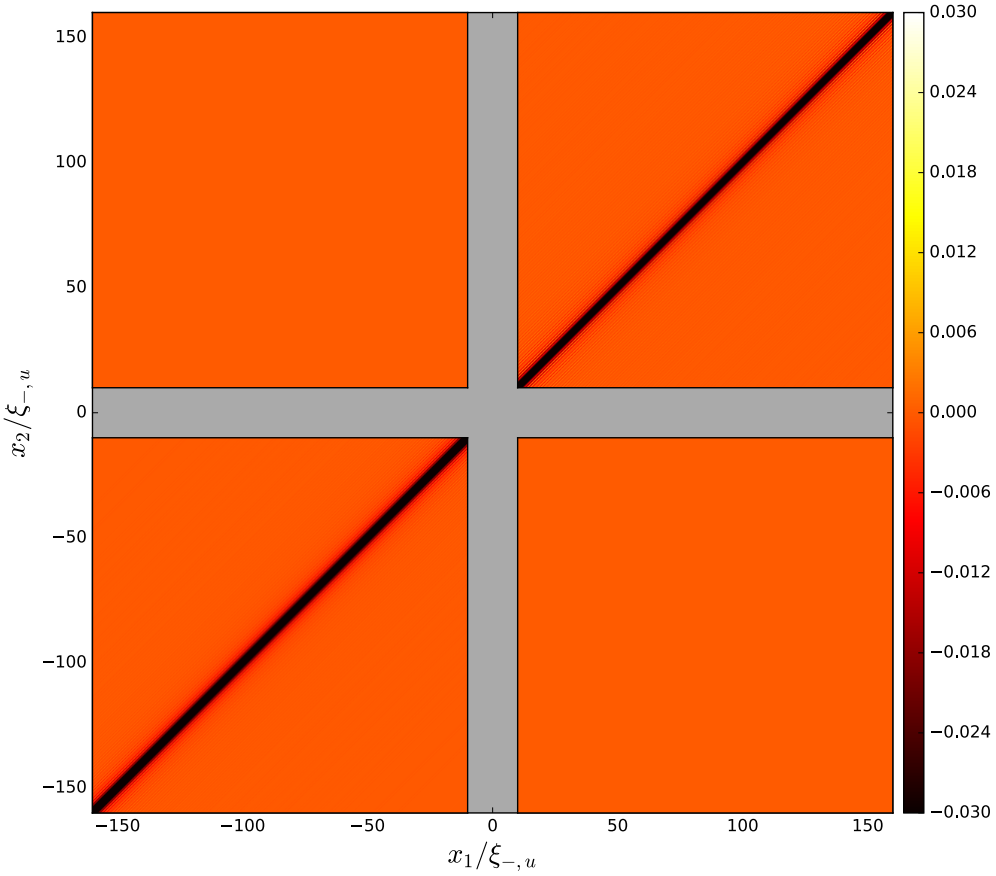

Figure 3.1: Plot for the dimensionless quantity $\xi_{-,u} g_+^{(2)}/2n_0$ with $\alpha_u = 0.2$, $J_{u,d} = 0$, $v/c_{+,u} = 0.572$ and $v/c_{+,d} = 0.448$. The shaded area near the axis corresponds to the zone $|x_1|, |x_2| < 10\xi_{-,u}$.

$$g_-^{(2)}(x_1, x_2) = 4n_0 \left\langle \delta\tilde{n}_-(x_1, t)\, \delta\tilde{n}_-(x_2, t) \right\rangle - 2n_0 \delta(x_1 - x_2), \tag{3.19}$$

where we used (3.3b).
With the decomposition (2.69a) equation (3.19) can be recast into

$$g_-^{(2)}(x_1, x_2) = 4\frac{n_0}{2} \int_0^\infty \frac{d\omega}{2\pi} \gamma_-(x_1, x_2, \omega) - 2n_0 \delta(x_1 - x_2). \tag{3.20}$$

Again we split $\gamma_-(x_1, x_2, \omega)$ and accordingly $g_-^{(2)}(x_1, x_2)$ into a zero-temperature term

$\gamma_{-,0}(x_1,x_2,\omega)$ and a thermal one $\gamma_{-,\mathrm{th}}(x_1,x_2,\omega)$. The zero-temperature contribution is

$$\gamma_{-,0}(x_1,x_2,\omega)=\sum_{L\in\{U,D1\}} f^{+}_{-,L}(x_1)\left(f^{+}_{-,L}(x_2)\right)^{*}+\left(f^{+}_{-,D2}(x_1)\right)^{*} f^{+}_{-,D2}(x_2)\,, \tag{3.21}$$

and the thermal one is

$$\begin{aligned}\gamma_{-,\mathrm{th}}(x_1,x_2,\omega)=\sum_{L\in\{U,D1,D2\}} &\Big[f^{+}_{-,L}(x_1)\left(f^{+}_{-,L}(x_2)\right)^{*}\\ &+\left(f^{+}_{-,L}(x_1)\right)^{*} f^{+}_{-,L}(x_2)\Big]\times\left\langle \hat{b}^{\dagger}_{L}(\omega)\,\hat{b}_{L}(\omega)\right\rangle .\end{aligned} \tag{3.22}$$

3.2.1 Density correlations with a gapless dispersion relation

In the following we will give the explicit expressions for $\gamma_{-,0}(x_1,x_2,\omega)$ for a configuration with a gapless dispersion relation. Again we will restrict ourselves to the case where x_1 and x_2 are both far from the horizon.

1. Case: x_1 and x_2 are both deep in the upstream region, $x_1,x_2\ll-\xi_{-,u}$

$$\begin{aligned}\gamma_{-,0}(x_1,x_2,\omega)=&\left|F^{+}_{-,u|\mathrm{in}}\right|^2 e^{ik_{u|\mathrm{in}}(x_1-x_2)}\\ &+\left|F^{+}_{-,u|\mathrm{out}}\right|^2 e^{ik_{u|\mathrm{out}}(x_1-x_2)}\\ &+\Theta(\Omega^{*}-\omega)\Big[\left|S^{-}_{u,d2}\right|^2\left|F^{+}_{-,u|\mathrm{out}}\right|^2 e^{ik_{u|\mathrm{out}}(x_1-x_2)}\\ &+c.c.\Big],\end{aligned} \tag{3.23}$$

where we used

$$\left|S^{-}_{u,u}\right|^2+\left|S^{-}_{u,d1}\right|^2=1+\Theta(\Omega^{*}-\omega)\left|S^{-}_{u,d2}\right|^2, \tag{3.24}$$

which comes from the η-unitarity (2.63) of the scattering matrix (2.62).

2. Case: x_1 is deep in the upstream region, x_2 deep in the downstream region, $x_1 \ll -\xi_{-,u}$ and $x_2 \gg \xi_{-,d}$

$$\begin{aligned}\gamma_{-,0}\left(x_1, x_2, \omega\right) = \\ \Theta\left(\Omega^* - \omega\right) \Big[& S^-_{u,d2} \left(S^-_{d1,d2}\right)^* F^+_{-,u|\mathrm{out}} \left(F^+_{-,d1|\mathrm{out}}\right)^* e^{i\left(k_{u|\mathrm{out}} x_1 - k_{d1|\mathrm{out}} x_2\right)} \\ & + S^-_{u,d2} \left(S^-_{d2,d2}\right)^* F^+_{-,u|\mathrm{out}} \left(F^+_{-,d2|\mathrm{out}}\right)^* e^{i\left(k_{u|\mathrm{out}} x_1 - k_{d2|\mathrm{out}} x_2\right)} \\ & + c.c.\Big] ,\end{aligned} \tag{3.25}$$

where we used

$$S^-_{u,u} \left(S^-_{d1,u}\right)^* + S^-_{u,d1} \left(S^-_{d1,d1}\right)^* = \Theta\left(\Omega^* - \omega\right) S^-_{u,d2} \left(S^-_{d1,d2}\right)^* , \tag{3.26a}$$

$$S^-_{u,u} \left(S^-_{d2,u}\right)^* + S^-_{u,d1} \left(S^-_{d2,d1}\right)^* = \Theta\left(\Omega^* - \omega\right) S^-_{u,d2} \left(S^-_{d2,d2}\right)^* . \tag{3.26b}$$

3. Case: x_1 is deep in the downstream region, x_2 deep in the upstream region, $x_1 \gg \xi_{-,d}$ and $x_2 \ll -\xi_{-,u}$

To obtain the expression for this case, it actually suffices to exchange the roles of x_1 and x_2 in the above formula (3.25).

$$\begin{aligned}\gamma_{-,0}\left(x_1, x_2, \omega\right) = \\ \Theta\left(\Omega^* - \omega\right) \Big[& S^-_{d1,d2} \left(S^-_{u,d2}\right)^* F^+_{-,d1|\mathrm{out}} \left(F^+_{-,u|\mathrm{out}}\right)^* e^{i\left(k_{d1|\mathrm{out}} x_1 - k_{u|\mathrm{out}} x_2\right)} \\ & + S^-_{d2,d2} \left(S^-_{u,d2}\right)^* F^+_{-,d2|\mathrm{out}} \left(F^+_{-,u|\mathrm{out}}\right)^* e^{i\left(k_{d2|\mathrm{out}} x_1 - k_{u|\mathrm{out}} x_2\right)} \\ & + c.c.\Big] ,\end{aligned} \tag{3.27}$$

which can be also obtained by using the complex conjugate of the relations (3.26).

4. Case: x_1 and x_2 are both deep in the downstream region, $x_1, x_2 \gg \xi_{-,d}$

$$\begin{aligned}
\gamma_{-,0}(x_1,x_2,\omega) = & \\
&+\left|F^{+}_{-,d1|\mathrm{in}}\right|^2 e^{ik_{d1|\mathrm{in}}(x_1-x_2)} \\
&+\left|F^{+}_{-,d1|\mathrm{out}}\right|^2 e^{ik_{d1|\mathrm{out}}(x_1-x_2)} \\
+\Theta(\Omega^*-\omega)&\Big[\left|F^{+}_{-,d2|\mathrm{in}}\right|^2 e^{-ik_{d2|\mathrm{in}}(x_1-x_2)} \\
&-\left|F^{+}_{-,d2|\mathrm{out}}\right|^2 e^{ik_{d2|\mathrm{out}}(x_1-x_2)}\Big] \\
+\Theta(\Omega^*-\omega)&\Big[\left|S^{-}_{d1,d2}\right|^2\left|F^{+}_{-,d1|\mathrm{out}}\right|^2 e^{ik_{d1|\mathrm{out}}(x_1-x_2)} \\
&+\left|S^{-}_{d2,d2}\right|^2\left|F^{+}_{-,d2|\mathrm{out}}\right|^2 e^{ik_{d2|\mathrm{out}}(x_1-x_2)} \\
&+S^{-}_{d1,d2}\left(S^{-}_{d2,d2}\right)^* F^{+}_{-,d1|\mathrm{out}}\left(F^{+}_{-,d2|\mathrm{out}}\right)^* e^{i\left(k_{d1|\mathrm{out}}x_1-k_{d2|\mathrm{out}}x_2\right)} \\
&+S^{-}_{d2,d2}\left(S^{-}_{d1,d2}\right)^* F^{+}_{-,d2|\mathrm{out}}\left(F^{+}_{-,d1|\mathrm{out}}\right)^* e^{i\left(k_{d2|\mathrm{out}}x_1-k_{d1|\mathrm{out}}x_2\right)} \\
&+c.c.\Big],
\end{aligned} \tag{3.28}$$

where we used

$$\left|S^{-}_{d1,u}\right|^2+\left|S^{-}_{d1,d1}\right|^2 = 1+\Theta(\Omega^*-\omega)\left|S^{-}_{d1,d2}\right|^2, \tag{3.29a}$$

$$\left|S^{-}_{d2,u}\right|^2+\left|S^{-}_{d2,d1}\right|^2 = -1+\left|S^{-}_{d2,d2}\right|^2, \tag{3.29b}$$

$$S^{-}_{d1,u}\left(S^{-}_{d2,u}\right)^*+S^{-}_{d1,d1}\left(S^{-}_{d2,d1}\right)^* = S^{-}_{d1,d2}\left(S^{-}_{d2,d2}\right)^*, \tag{3.29c}$$

and the complex conjugate of relation (3.29c).

In contrast to the symmetric degrees of freedom, the correlation signal for the anti-symmetric degrees of freedom is not only modified because of the different healing lengths $\xi_{-,u}$ and $\xi_{-,d}$ in the upstream and downstream region respectively but also new long-range correlations appear, which can be interpreted as emission of correlated phonons. These correlated phonons are generated by quantum fluctuations and propagate away from the horizon in the $u|$out, $d1|$out and $d2|$out channels. In the low ω limit the velocities with which the phonons propagete away from the horizon can be approximated by $v_{u|\mathrm{out}} = v - c_{-,u}$, $v_{d1|\mathrm{out}} = v + c_{-,d}$ and $v_{d2|\mathrm{out}} = v - c_{-,d}$. Thus at

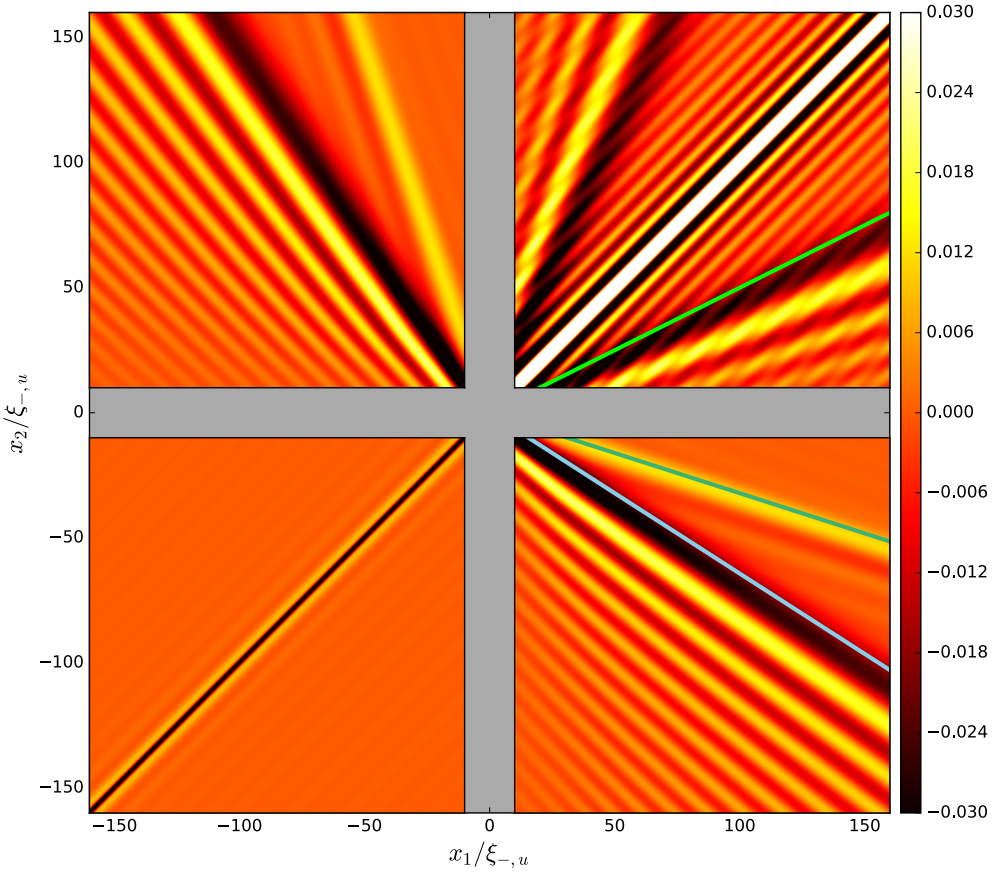

Figure 3.2: Plot for the dimensionless quantity $\xi_{-,u} g_{-}^{(2)}/2n_0$ with $\alpha_u = 0.2$, $J_{u,d} = 0$, $v/c_{+,u} = 0.7$ and $v/c_{+,d} = 3$. The shaded area near the axis corresponds to the zone $|x_1|, |x_2| < 10\xi_{-,u}$. The straight lines correspond to the correlation lines where the largest long-range signal is expected. The lime-green line corresponds to the $d2 - d1$ correlations, the seagreen one to the $u - d1$ correlations and the lightblue one to the $u - d2$ correlations.

time t after their emission, these phonons are respectively located at $(v - c_{-,u})\, t < 0$, $(v + c_{-,d})\, t > 0$ and $(v - c_{-,d})\, t > 0$. Therefore we expect a correlation signal along lines of slope $(v - c_{-,u}) / (v + c_{-,d})$ resulting from correlations between phonons emitted along the $u|$out and $d1|$out channels, $(v - c_{-,u}) / (v - c_{-,d})$ for correlated phonons emitted along the $u|$out and $d2|$out channels and $(v - c_{-,d}) / (v + c_{-,d})$ for correlated phonons emitted along the $d1|$out and $d2|$out channels. We also expect a correlation

signal along lines of inverse slope, which correspond to the exchange $x_1 \longleftrightarrow x_2$.

In figure 3.2 we plotted the quantity $\xi_{-,u} g_-^{(2)}/2n_0$ in a configuration where a black hole horizon only occurs in the anti-symmetric regime. We set $\alpha_u = 0.2$, $J_{u,d} = 0$, $v/c_{-,u} = 0.7$ and $v/c_{-,d} = 3$. The numerical integration was cut off at $80\Omega^*$, which corresponds to $8.968\mu_u$ and $5.816\mu_d$. We only plotted the correlation functions for $|x_1|, |x_2| > 10\xi_{-,u}$, that is the region, where equations (3.23), (3.25), (3.27) and (3.28) are valid. The three slopes where we expected the largest long-range correlation signal are marked by solid lines. The actual large-distance correlation lines correspond very well to the expected ones.

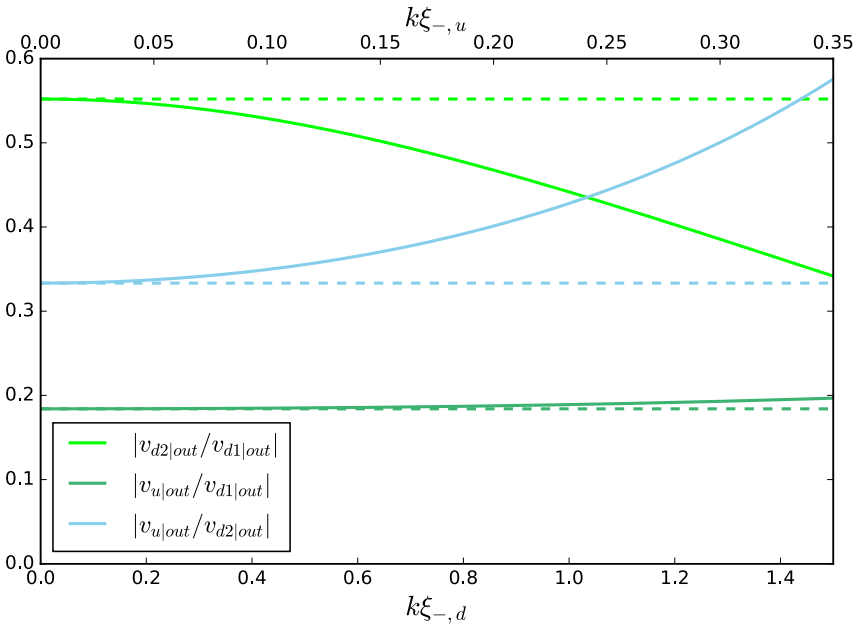

Figure 3.3: Comparison of the slopes of the correlation lines in the low ω limit with the exact ratio of the k-dependent velocities for a gapless dispersion relation. Approximated values are represented by dashed lines, exact values by straight lines. The lower x-axis shows k in units of inverse healing lengths of the downstream region, the upper x-axis shows k in units of inverse healing lengths of the upstream region.

In figure 3.3 we compared $v_{u|\mathrm{out}}/v_{d1|\mathrm{out}}$, $v_{u|\mathrm{out}}/v_{d2|\mathrm{out}}$ and $v_{d2|\mathrm{out}}/v_{d1|\mathrm{out}}$ in the low ω limit with their actual k-dependent values, where $v_\ell = d\omega/dk_\ell$ with $\ell \in \{u|\mathrm{out}, d1|\mathrm{out}, d2|\mathrm{out}\}$. For small k they fit remarkably well, though for $k = \xi_{-,d}^{-1}$ the deviation of the actual value from the approximated one is 19.99% for $v_{d2|\mathrm{out}}/v_{d1|\mathrm{out}}$, 28.39% for $v_{u|\mathrm{out}}/v_{d2|\mathrm{out}}$ and

2.84% for $v_{u|\mathrm{out}}/v_{d1|\mathrm{out}}$. Close to $k^* = 3.427\xi_{-,d}^{-1}$, which is the k corresponding to Ω^*, the deviation is even larger. The nevertheless good correspondence of the approximated locations of the largest long-range correlation signals indicates that the Hawking signal is dominated by modes with small k, that is low ω modes. This is due to the fact that the transmission and reflection coefficients for a $d1$ or $d2$ ingoing mode diverge in the low ω limit as can be seen in figure 2.9.

Now we consider a configuration with a non-zero tunnel coupling J, but with a gapless dispersion relation. This is the case, when $2gn_0\left(1-\alpha_{u,d}\right)+2J_{u,d}=0$ in the dispersion relation (2.16b). This gives us

$$J_{u,d} = gn_0\left(\alpha_{u,d}-1\right). \tag{3.30}$$

The velocities of sound can now be written as

$$c_{-,u,d}^2 = \frac{J_{u,d}}{m} = \frac{gn_0\left(\alpha_{u,d}-1\right)}{m}. \tag{3.31}$$

In order for $c_{-,u}$ and $c_{-,d}$ to be real valued, we need $\alpha_{u,d} > 1$.

In figure 3.4 we plotted the quantity $\xi_{-,u}g_-^{(2)}/2n_0$ in such a configuration. We set $\alpha_u = 1.2$, $v/c_{+,u} = 0.7$, $v/c_{+,d} = 3$ and calculated $J_{u,d}$ according to equation (3.30). The numerical integration was cut of at $300\Omega^*$, which corresponds to $0.585\mu_{u,d}$. Again, we only plotted the correlation function for $|x_1|, |x_2| > 10\xi_{-,u}$. The low ω approximation of $v_{u|\mathrm{out}}$, $v_{d1|\mathrm{out}}$ and $v_{d2|\mathrm{out}}$ leads to the same results as the above $J_{u,d} = 0$ case. Therefore the formulas for the slopes of the expected correlation lines are identical. In the Plot we see, that the actual large-distance correlation lines again correspond very well to the expected one.
Due to the fact that we chose $v/c_{+,u} = 0.7$ and $v/c_{+,d} = 3$ just as in the above case, figure 3.3 is also valid for our present configuration. So also in this case, the Hawking signal is dominated by low ω modes. Here too, the transmission and reflection coefficients for a $d1$ or $d2$ ingoing mode diverge in the low ω limit.

3.2.2 Density correlations with a gaped dispersion relation

In this section we will consider the density correlations of a configuration with a dispersion relation containing a small gap. The explicit expressions can be obtained by replacing each u in expressions (3.23), (3.25) and (3.27) by $u1$ and multiplying each of

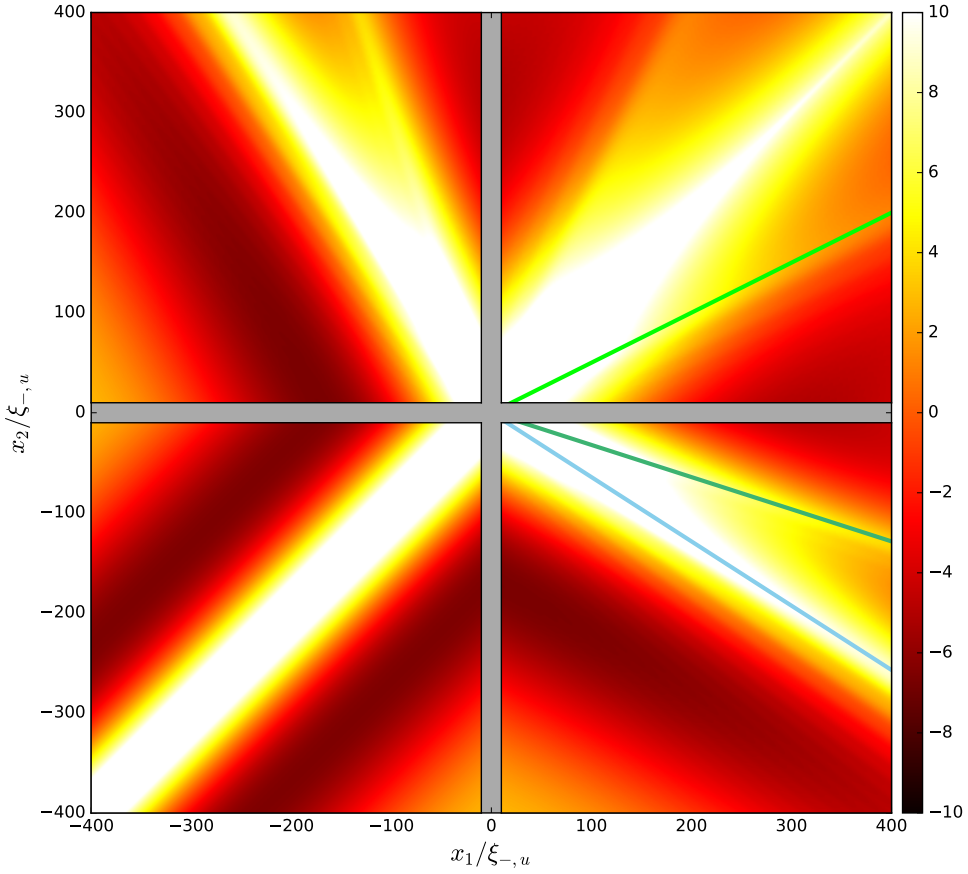

Figure 3.4: Plot for the dimensionless quantity $\xi_{-,u} g_-^{(2)}/2n_0$ with $\alpha_u = 1.2$, $v/c_{+,u} = 0.7$ and $v/c_{+,d} = 3$. $J_{u,d}$ are calculated according to (3.30). The shaded area near the axis corresponds to the zone $|x_1|, |x_2| < 10\xi_{-,u}$. The straight lines correspond to the correlation lines where the largest long-range signal is expected. The lime-green line corresponds to the $d2-d1$ correlations, the seagreen one to the $u-d1$ correlations and the lightblue one to the $u-d2$ correlations.

them with $\Theta(\omega - \omega^*)$. Expression (3.28) is the same for a gaped dispersion relation as for a gapless.

Due to the gap the quasi-particles get an effective mass proportional to ω_0 which is defined in equation (2.17). Comparing equation (2.17) with the dispersion relation (2.16b) gives us

$$\omega_{0,u,d}^2 = 4J_{u,d}\left[gn_0\left(1-\alpha_{u,d}\right)+J_{u,d}\right]. \tag{3.32}$$

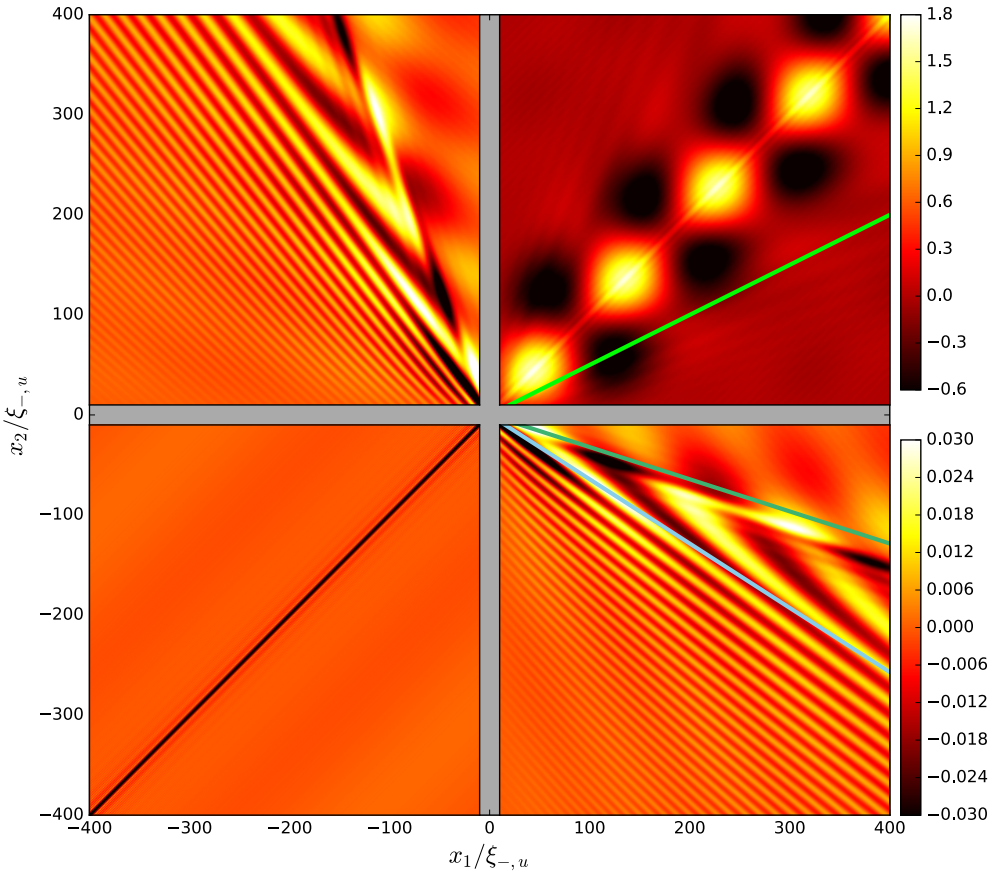

Figure 3.5: Plot for the dimensionless quantity $\xi_{-,u}g_{-}^{(2)}/2n_0$ with $\alpha_u = 0.2$, $J_u/gn_0 = 10^{-4}$, $v/c_{+,u} = 0.7$ and $v/c_{+,d} = 3$. The shaded area near the axis corresponds to the zone $|x_1|, |x_2| < 10\xi_{-,u}$. The straight lines correspond to the correlation lines where the largest long-range signal would be expected in case of a gapless dispersion relation. The lime-green line corresponds to the $d2-d1$ correlations, the seagreen one to the $u-d1$ correlations and the lightblue one to the $u-d2$ correlations.

The quasi-particles should have a constant effective mass throughout the whole system, thus we require

$$\omega_0^2 = 4J_u \left[gn_0 \left(1-\alpha_u\right) + J_u\right] = 4J_d \left[gn_0 \left(1-\alpha_d\right) + J_d\right]. \tag{3.33}$$

The correlation signal in this configuration is modified because of the different healing lengths ξ_{-u}, and $\xi_{-,d}$ in the upstream and downstream region respectively and also long-range correlations are expected, which can be interpreted as emission of correlated quasi-particles propagating away from the horizon in the $u|$out, $d1|$out and $d2|$out channels. Though this time the $u|$out channel only exists for $\omega > \omega^*$.

In figures 3.5 and 3.6 we plotted the quantity $\xi_{-,u} g_-^{(2)}/2n_0$ for a configuration with a gaped dispersion relation with $\alpha_u = 0.2$, $v/c_{+,u} = 0.7$, $v/c_{+,d} = 3$, $J_u/gn_0 = 10^{-4}$ and $J_u/gn_0 = 10^{-5}$ respectively. In both cases the numerical integration was cut off at $30\Omega^*$, which corresponds to $3.349\mu_u$ and $2.170\mu_d$ for figure 3.5 and to $3.362\mu_u$ and $2.180\mu_d$ for figure 3.6. Again, we only plotted the correlation function for $|x_1|, |x_2| > 10\xi_{-,u}$. Due to the gap the above approximation for $v_{u|\mathrm{out}}$, $v_{d1|\mathrm{out}}$ and $v_{d2|\mathrm{out}}$ is not valid anymore. As can be seen in the plots, the slopes of the above approximation only correspond very roughly to the actual signal. However we still find a Hawking-like signal.
In figure 3.7 we compare the $v_{u|\mathrm{out}}/v_{d1|\mathrm{out}}$, $v_{u|\mathrm{out}}/v_{d2|\mathrm{out}}$ and $v_{d2|\mathrm{out}}/v_{d1|\mathrm{out}}$ in the low ω limit for a gapless dispersion relation with the actual k-dependent values for the gaped dispersion relations. As expected the correspondence is not good in any case, although it is a little bit better for the lower plot with $J_{-,u}/gn_0 = 10^{-5}$. This is because $J_{-,u} \to 0$ would close the gap and restore figure 3.2.

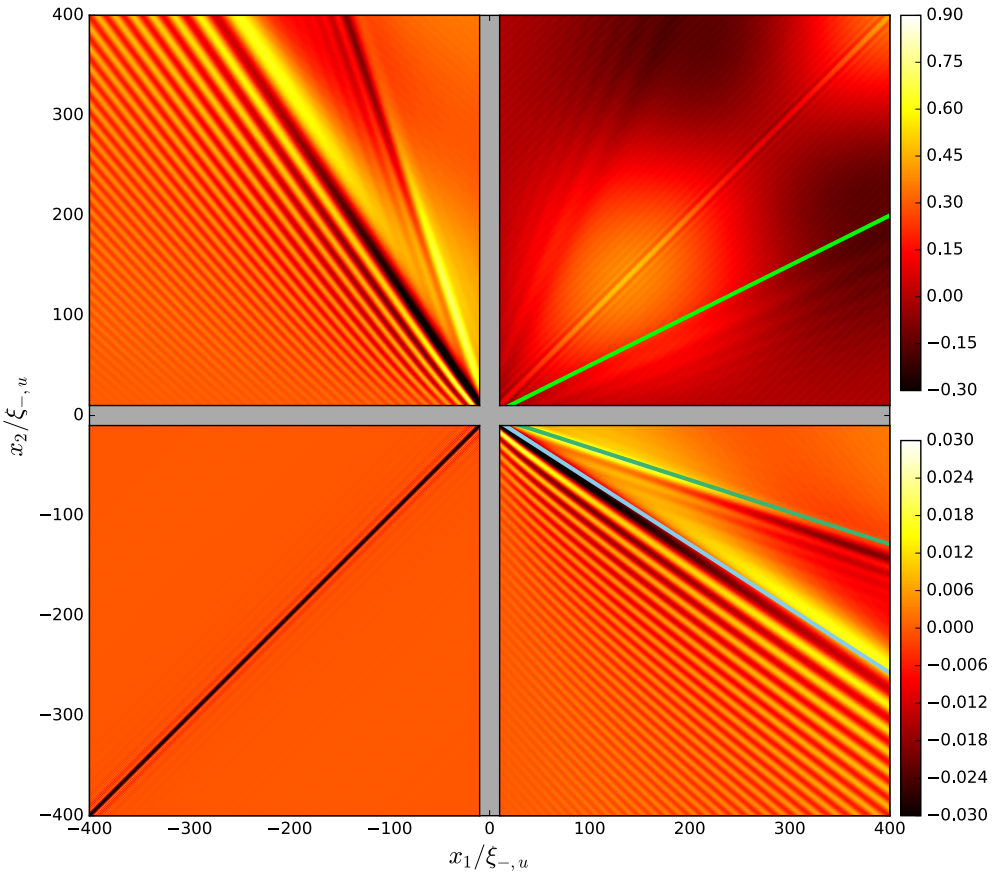

Figure 3.6: Plot for the dimensionless quantity $\xi_{-,u} g_-^{(2)}/2n_0$ with $\alpha_u = 0.2$, $J_u/gn_0 = 10^{-5}$, $v/c_{+,u} = 0.7$ and $v/c_{+,d} = 3$. The shaded area near the axis corresponds to the zone $|x_1|, |x_2| < 10\xi_{-,u}$. The straight lines correspond to the correlation lines where the largest long-range signal would be expected in case of a gapless dispersion relation. The lime-green line corresponds to the $d2-d1$ correlations, the seagreen one to the $u-d1$ correlations and the lightblue one to the $u-d2$ correlations.

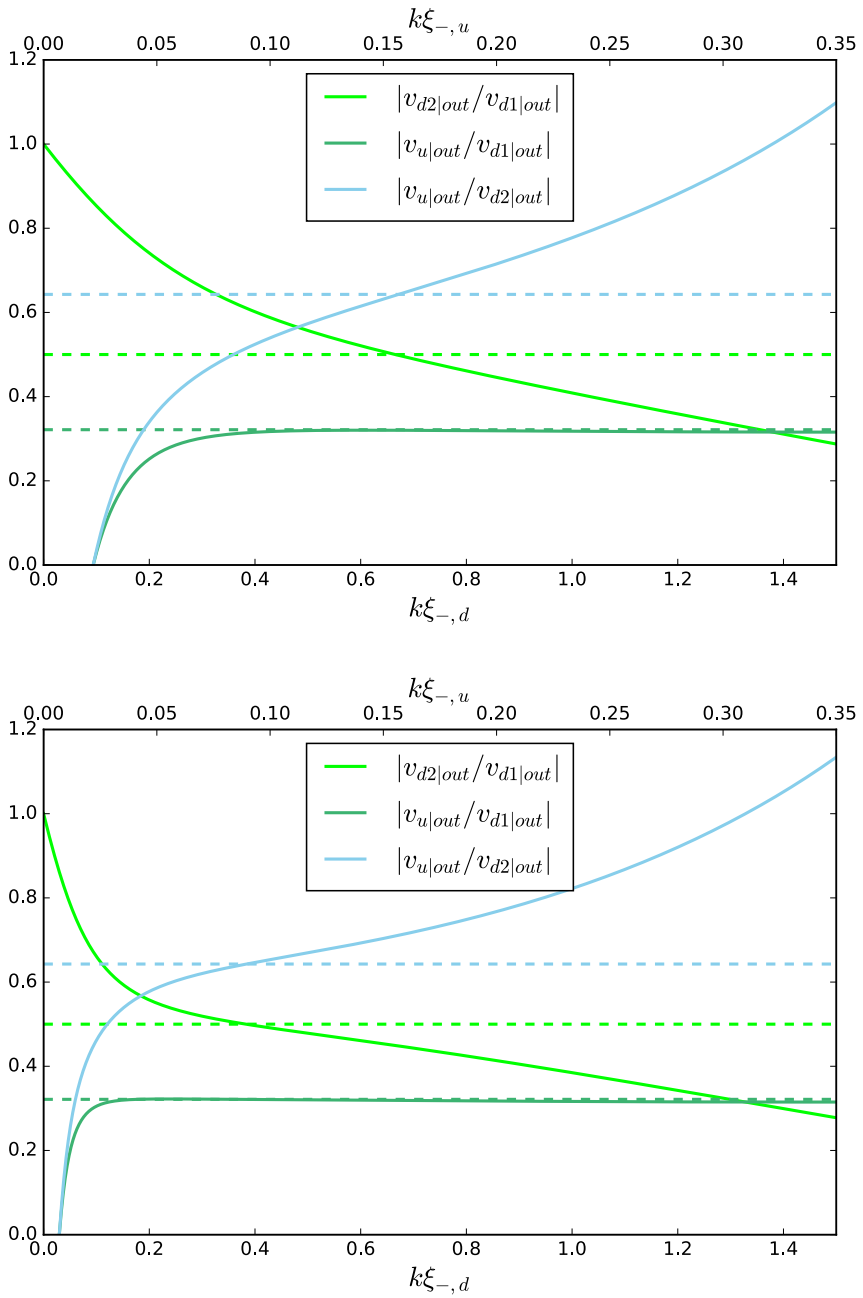

Figure 3.7: Comparison of the slopes of the correlation lines in the low ω limit as expected in a gapless configuration with the exact ratio of the k-dependent velocities for a gaped dispersion relation. The above panel corresponds to the parameters in figure 3.5, the lower panel to the parameters in figure 3.6. Approximated values are represented by dashed lines, exact values by straight line. The lower x-axis shows k in units of inverse healing lengths of the downstream region, the upper x-axis shows k in units of inverse healing lengths of the upstream region.

4 Conclusion

In this thesis we considered a one-dimensional two-component Bose Einstein condensate with a background flow that is transsonic in the anti-symmetric degrees of freedom but remains subsonic throughout the whole system in the symmetric degrees of freedom. The point of the transition from a subsonic upstream region to a supersonic downstream region acts as the sonic analogue of en event horizon. We found that in the symmetric degrees of freedom the two-point density correlator is modified compared to the correlator for a homogeneous configuration. This modifications only affect the short-range correlation signal and are due to the different healing lengths on the upstream and downstream side of the horizon. The modifications in the symmetric degrees of freedom are not affected by the horizon in the anti-symmetric degrees of freedom.
In the anti-symmetric degrees of freedom with no tunnel coupling there is another modification corresponding to long-distance correlations, which can be interpreted as the emission of correlated phonons. Our predictions of the location of the strongest long-distance correlation signals which appear as a consequence of the Hawking emission are in good agreement with our numerical calculations. The fact that these correlation signals only appear in the anti-symmetric degrees of freedom but not in the symmetric ones is an evidence that they are indeed intrinsically connected to Hawking radiation and require the occurrence of a horizon. In this configuration all our results are in accordance with the results in [31, 32]. For a discussion about the experimental realisation of such a configuration also see [31].
In a configuration with non-zero tunnel coupling J but a gapless dispersion relation, the equations for the density correlation function are equal to the equations in the configuration with zero tunnel coupling. The long-distance correlation signal are also present in this configuration. Here, too, we find our numerical calculations to be in good agreement with our predictions of the location of the strongest long-distance correlation signals. However an experimental realisation of this configuration might be tricky since, in order to keep the dispersion relation gapless, it is exactly at a phase transition.
The last configuration we considered was one with a gaped dispersion relation. This gap gives our quasi-particles an effective mass which strongly affects the frequency range

for which the long-distance correlation signals occur. Nevertheless if we choose our parameters such that $\omega^* < \Omega^*$ we again find the characteristic Hawking-like long-distance correlation signals. Though due to the effective mass of our quasi-particles it is not possible to make a good prediction of the location of these correlation signals. So in this configuration we find a kind of massive Hawking effect, which is not only interesting from the gravitational analogy point of view.
In all three configurations we used a step-like background which is not at all realistic. Though our approach can easily be extended for more experimentally realisable configurations as has been done for a one-component Bose gas in [28].

References

[1] S. W. Hawking. "Black hole explosion?" In: *Nature* 248.5443 (1974), pp. 30–31. DOI: 10.1038/248030a0. URL: http://dx.doi.org/10.1038/248030a0.

[2] S. W. Hawking. "Particle creation by black holes". In: *Communications in Mathematical Physics* 43.3 (1975), pp. 199–220. ISSN: 1432-0916. DOI: 10.1007/BF02345020. URL: http://dx.doi.org/10.1007/BF02345020.

[3] B. Carr and S.W. Hawking. "Black holes in the early Universe". In: *Mon. Not. Roy. Astron. Soc.* 168 (1974), pp. 399–415.

[4] W. G. Unruh. "The Analogue Between Rimfall and Black Holes". In: *Quantum Analogues: From Phase Transitions to Black Holes and Cosmology*. Ed. by William G. Unruh and Ralf Schützhold. Berlin, Heidelberg: Springer Berlin Heidelberg, 2007, pp. 1–4. ISBN: 978-3-540-70859-9. DOI: 10.1007/3-540-70859-6_1. URL: http://dx.doi.org/10.1007/3-540-70859-6_1.

[5] Germain Rousseaux et al. "Observation of negative-frequency waves in a water tank: a classical analogue to the Hawking effect?" In: *New Journal of Physics* 10.5 (2008), p. 053015. URL: http://stacks.iop.org/1367-2630/10/i=5/a=053015.

[6] Silke Weinfurtner et al. "Measurement of Stimulated Hawking Emission in an Analogue System". In: *Phys. Rev. Lett.* 106 (2 Jan. 2011), p. 021302. DOI: 10.1103/PhysRevLett.106.021302. URL: http://link.aps.org/doi/10.1103/PhysRevLett.106.021302.

[7] W. G. Unruh. "Sonic analogue of black holes and the effects of high frequencies on black hole evaporation". In: *Phys. Rev. D* 51 (6 Mar. 1995), pp. 2827–2838. DOI: 10.1103/PhysRevD.51.2827. URL: http://link.aps.org/doi/10.1103/PhysRevD.51.2827.

[8] Thomas G. Philbin et al. "Fiber-Optical Analog of the Event Horizon". In: *Science* 319.5868 (2008), pp. 1367–1370. ISSN: 0036-8075. DOI: 10.1126/science.1153625. eprint: http://science.sciencemag.org/content/319/5868/1367.full.pdf. URL: http://science.sciencemag.org/content/319/5868/1367.

[9] F. Belgiorno et al. “Hawking Radiation from Ultrashort Laser Pulse Filaments”. In: *Phys. Rev. Lett.* 105 (20 Nov. 2010), p. 203901. DOI: 10.1103/PhysRevLett.105.203901. URL: http://link.aps.org/doi/10.1103/PhysRevLett.105.203901.

[10] M. Elazar, V. Fleurov, and S. Bar-Ad. “All-optical event horizon in an optical analog of a Laval nozzle”. In: *Phys. Rev. A* 86 (6 Dec. 2012), p. 063821. DOI: 10.1103/PhysRevA.86.063821. URL: http://link.aps.org/doi/10.1103/PhysRevA.86.063821.

[11] B. Horstmann et al. “Hawking Radiation from an Acoustic Black Hole on an Ion Ring”. In: *Phys. Rev. Lett.* 104 (25 June 2010), p. 250403. DOI: 10.1103/PhysRevLett.104.250403. URL: http://link.aps.org/doi/10.1103/PhysRevLett.104.250403.

[12] Ralf Schützhold and William G. Unruh. “Hawking Radiation in an Electromagnetic Waveguide?” In: *Phys. Rev. Lett.* 95 (3 July 2005), p. 031301. DOI: 10.1103/PhysRevLett.95.031301. URL: http://link.aps.org/doi/10.1103/PhysRevLett.95.031301.

[13] Alfredo Iorio and Gaetano Lambiase. “The Hawking–Unruh phenomenon on graphene”. In: *Physics Letters B* 716.2 (2012), pp. 334–337. ISSN: 0370-2693. DOI: http://dx.doi.org/10.1016/j.physletb.2012.08.023. URL: http://www.sciencedirect.com/science/article/pii/S037026931200860X.

[14] PISIN CHEN and HARET ROSU. “NOTE ON HAWKING–UNRUH EFFECTS IN GRAPHENE”. In: *Modern Physics Letters A* 27.37 (2012), p. 1250218. DOI: 10.1142/S0217732312502185. eprint: http://www.worldscientific.com/doi/pdf/10.1142/S0217732312502185. URL: http://www.worldscientific.com/doi/abs/10.1142/S0217732312502185.

[15] Michael Stone. “An analogue of Hawking radiation in the quantum Hall effect”. In: *Classical and Quantum Gravity* 30.8 (2013), p. 085003. URL: http://stacks.iop.org/0264-9381/30/i=8/a=085003.

[16] L. J. Garay et al. “Sonic Analog of Gravitational Black Holes in Bose-Einstein Condensates”. In: *Phys. Rev. Lett.* 85 (22 Nov. 2000), pp. 4643–4647. DOI: 10.1103/PhysRevLett.85.4643. URL: http://link.aps.org/doi/10.1103/PhysRevLett.85.4643.

[17] Carlos Barceló, Stefano Liberati, and Matt Visser. “Towards the Observation of Hawking Radiation in Bose–Einstein Condensates”. In: *International Journal of Modern Physics A* 18.21 (2003), pp. 3735–3745. DOI: 10.1142/S0217751X0301615X.

eprint: http://www.worldscientific.com/doi/pdf/10.1142/S0217751X0301615X. URL: http://www.worldscientific.com/doi/abs/10.1142/S0217751X0301615X.

[18] Carlos Barceló, S. Liberati, and Matt Visser. "Probing semiclassical analog gravity in Bose-Einstein condensates with widely tunable interactions". In: *Phys. Rev. A* 68 (5 Nov. 2003), p. 053613. DOI: 10.1103/PhysRevA.68.053613. URL: http://link.aps.org/doi/10.1103/PhysRevA.68.053613.

[19] S. Giovanazzi et al. "Conditions for one-dimensional supersonic flow of quantum gases". In: *Phys. Rev. A* 70 (6 Dec. 2004), p. 063602. DOI: 10.1103/PhysRevA.70.063602. URL: http://link.aps.org/doi/10.1103/PhysRevA.70.063602.

[20] Carlos Barceló, Stefano Liberati, and Matt Visser. "Analogue Gravity". In: *Living Reviews in Relativity* 8.1 (2005), p. 12. ISSN: 1433-8351. DOI: 10.12942/lrr-2005-12. URL: http://dx.doi.org/10.12942/lrr-2005-12.

[21] Ralf Schützhold. "Detection Scheme for Acoustic Quantum Radiation in Bose-Einstein Condensates". In: *Phys. Rev. Lett.* 97 (19 Nov. 2006), p. 190405. DOI: 10.1103/PhysRevLett.97.190405. URL: http://link.aps.org/doi/10.1103/PhysRevLett.97.190405.

[22] S. Wüster and C. M. Savage. "Limits to the analog Hawking temperature in a Bose-Einstein condensate". In: *Phys. Rev. A* 76 (1 July 2007), p. 013608. DOI: 10.1103/PhysRevA.76.013608. URL: http://link.aps.org/doi/10.1103/PhysRevA.76.013608.

[23] Yasunari Kurita and Takao Morinari. "Formation of a sonic horizon in isotropically expanding Bose-Einstein condensates". In: *Phys. Rev. A* 76 (5 Nov. 2007), p. 053603. DOI: 10.1103/PhysRevA.76.053603. URL: http://link.aps.org/doi/10.1103/PhysRevA.76.053603.

[24] Roberto Balbinot et al. "Nonlocal density correlations as a signature of Hawking radiation from acoustic black holes". In: *Phys. Rev. A* 78 (2 Aug. 2008), p. 021603. DOI: 10.1103/PhysRevA.78.021603. URL: http://link.aps.org/doi/10.1103/PhysRevA.78.021603.

[25] S. Wüster. "Phonon background versus analog Hawking radiation in Bose-Einstein condensates". In: *Phys. Rev. A* 78 (2 Aug. 2008), p. 021601. DOI: 10.1103/PhysRevA.78.021601. URL: http://link.aps.org/doi/10.1103/PhysRevA.78.021601.

[26] A. Recati, N. Pavloff, and I. Carusotto. "Bogoliubov theory of acoustic Hawking radiation in Bose-Einstein condensates". In: *Phys. Rev. A* 80 (4 Oct. 2009), p. 043603. DOI: 10.1103/PhysRevA.80.043603. URL: http://link.aps.org/doi/10.1103/PhysRevA.80.043603.

[27] Jean Macher and Renaud Parentani. "Black-hole radiation in Bose-Einstein condensates". In: *Phys. Rev. A* 80 (4 Oct. 2009), p. 043601. DOI: 10.1103/PhysRevA.80.043601. URL: http://link.aps.org/doi/10.1103/PhysRevA.80.043601.

[28] P.-É. Larré et al. "Quantum fluctuations around black hole horizons in Bose-Einstein condensates". In: *Phys. Rev. A* 85 (1 Jan. 2012), p. 013621. DOI: 10.1103/PhysRevA.85.013621. URL: http://link.aps.org/doi/10.1103/PhysRevA.85.013621.

[29] D. D. Solnyshkov, H. Flayac, and G. Malpuech. "Black holes and wormholes in spinor polariton condensates". In: *Phys. Rev. B* 84 (23 Dec. 2011), p. 233405. DOI: 10.1103/PhysRevB.84.233405. URL: http://link.aps.org/doi/10.1103/PhysRevB.84.233405.

[30] Dario Gerace and Iacopo Carusotto. "Analog Hawking radiation from an acoustic black hole in a flowing polariton superfluid". In: *Phys. Rev. B* 86 (14 Oct. 2012), p. 144505. DOI: 10.1103/PhysRevB.86.144505. URL: http://link.aps.org/doi/10.1103/PhysRevB.86.144505.

[31] P.-É. Larré and N. Pavloff. "Hawking radiation in a two-component Bose-Einstein condensate". In: *EPL (Europhysics Letters)* 103.6 (2013), p. 60001. URL: http://stacks.iop.org/0295-5075/103/i=6/a=60001.

[32] P.-É. Larré. "Fluctuations quantiques et e ets non-linéaires dans les condensats de Bose-Einstein". 2013.

[33] Franco Dalfovo et al. "Theory of Bose-Einstein condensation in trapped gases". In: *Rev. Mod. Phys.* 71 (3 Apr. 1999), pp. 463–512. DOI: 10.1103/RevModPhys.71.463. URL: http://link.aps.org/doi/10.1103/RevModPhys.71.463.

[34] Oren Lahav et al. "Realization of a Sonic Black Hole Analog in a Bose-Einstein Condensate". In: *Phys. Rev. Lett.* 105 (24 Dec. 2010), p. 240401. DOI: 10.1103/PhysRevLett.105.240401. URL: http://link.aps.org/doi/10.1103/PhysRevLett.105.240401.

[35] Jeff Steinhauer. "Observation of quantum Hawking radiation and its entanglement in an analogue black hole". In: *Nature Physics* 12 (2016), pp. 959–965. DOI: doi:10.1038/nphys3863.

[36] Iacopo Carusotto et al. "Numerical observation of Hawking radiation from acoustic black holes in atomic Bose–Einstein condensates". In: *New Journal of Physics* 10.10 (2008), p. 103001. URL: http://stacks.iop.org/1367-2630/10/i=10/a=103001.

[37] S. Weinfurtner, S. Liberati, and M. Visser. "Analogue Space-time Based on 2-Component Bose-Einstein Condensates". In: *Quantum Analogues: From Phase Transitions to Black Holes and Cosmology*. Ed. by William G. Unruh and Ralf Schützhold. Berlin, Heidelberg: Springer Berlin Heidelberg, 2007, pp. 115–163. ISBN: 978-3-540-70859-9. DOI: 10.1007/3-540-70859-6_6. URL: http://dx.doi.org/10.1007/3-540-70859-6_6.

[38] S. Erne et al. "Generalized Gibbs Ensemble for two linearly coupled Quasicondensates". in preparation.

[39] Markus Karl. "From Quenches to Critical Dynamics and Non-Equilibrium Steady States: Universality in the Dynamics of Low-Dimensional Ultracold Bose Gases". 2016.

[40] W. G. Unruh. "Experimental Black-Hole Evaporation?" In: *Phys. Rev. Lett.* 46 (21 May 1981), pp. 1351–1353. DOI: 10.1103/PhysRevLett.46.1351. URL: http://link.aps.org/doi/10.1103/PhysRevLett.46.1351.

[41] Roberto Balbinot et al. "Understanding Hawking Radiation from Simple Models of Atomic Bose-Einstein Condensates". In: *Analogue Gravity Phenomenology: Analogue Spacetimes and Horizons, from Theory to Experiment*. Ed. by Daniele Faccio et al. Cham: Springer International Publishing, 2013, pp. 181–219. ISBN: 978-3-319-00266-8. DOI: 10.1007/978-3-319-00266-8_9. URL: http://dx.doi.org/10.1007/978-3-319-00266-8_9.

[42] Carlos Barceló, Stefano Liberati, and Matt Visser. "Analogue Gravity". In: *Living Reviews in Relativity* 14.1 (2011), p. 3. ISSN: 1433-8351. DOI: 10.12942/lrr-2011-3. URL: http://dx.doi.org/10.12942/lrr-2011-3.

[43] C. Barceló et al. "Stability analysis of sonic horizons in Bose-Einstein condensates". In: *Phys. Rev. D* 74 (2 July 2006), p. 024008. DOI: 10.1103/PhysRevD.74.024008. URL: http://link.aps.org/doi/10.1103/PhysRevD.74.024008.

[44] P. Deuar et al. "Nonlocal pair correlations in the one-dimensional Bose gas at finite temperature". In: *Phys. Rev. A* 79 (4 Apr. 2009), p. 043619. DOI: 10.1103/PhysRevA.79.043619. URL: http://link.aps.org/doi/10.1103/PhysRevA.79.043619.

Erklärung:

Ich versichere, dass ich diese Arbeit selbstständig verfasst habe und keine anderen als die angegebenen Quellen und Hilfsmittel benutzt habe.

Heidelberg, den (Datum) .....